Hearing the heat: a proof-of-concept study of nonlinear sound measures for distinguishing phases of rapid organic decomposition

Jakob Eisenhauer[a,*]

[a] Department of Earth and Environmental Sciences, Lund University, Sölvegatan 12, 223 62 Lund, Sweden

[*] **Corresponding author**
Jakob Eisenhauer
Email: jakob.eisenhauer.1533@student.lu.se
ORCID: 0009-0009-7121-0615

Preprint status

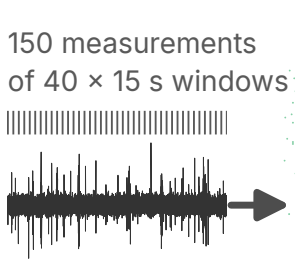
This manuscript is a **non-peer-reviewed preprint** submitted to EarthArXiv.

Listening to decomposition



5 buckets,
vermicompost & hay

150 measurements
of 40 × 15 s windows



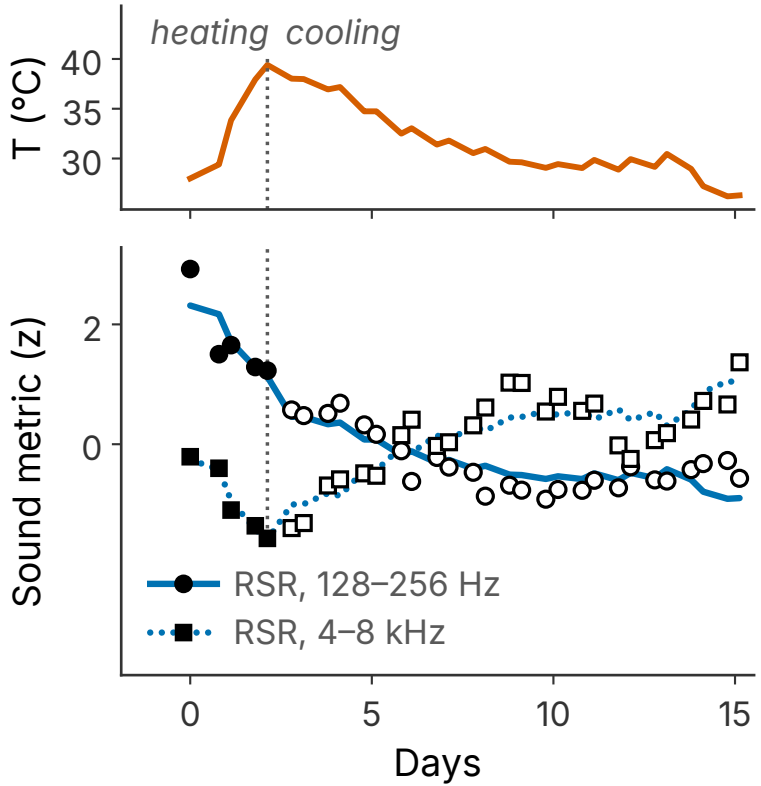


× 32 × 48

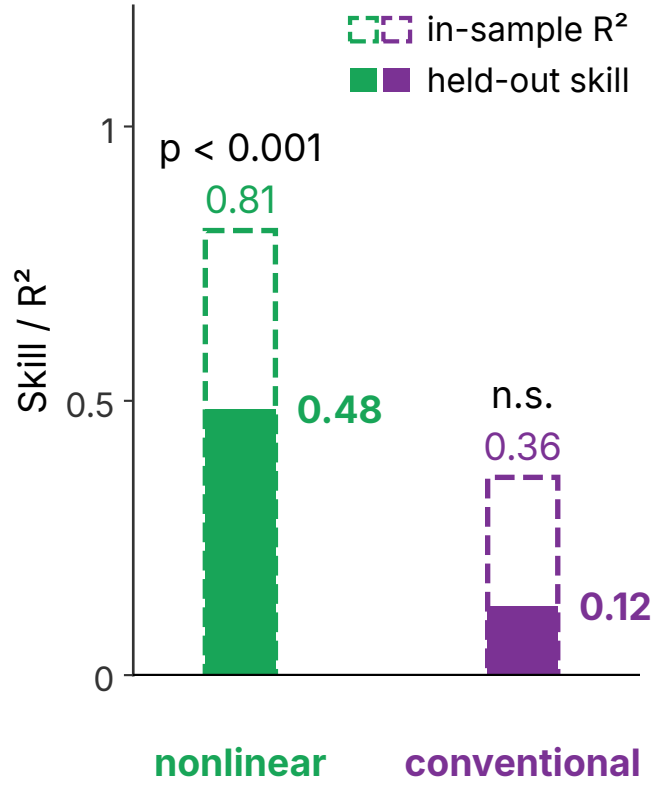
4 & **6** measures in 8 frequency bands

= 480 000 values

Sound tracks phases of rapid organic decomposition



Nonlinear measures predict unseen buckets



Hearing the heat: a proof-of-concept study of nonlinear sound measures for distinguishing phases of rapid organic decomposition

Jakob Eisenhauer[a,*]

[a]*Department of Earth and Environmental Sciences, Lund University, Sölvegatan 12, 223 62 Lund, Sweden*

Abstract

Acoustic recording can follow decomposition non-destructively, but which acoustic measures carry process information is largely untested. In a proof-of-concept experiment, four nonlinear complexity measures and six conventional ecoacoustic indices were compared in eight octave bands, using 150 recordings from five buckets of one vermicompost-hay batch during one mesophilic heating-cooling cycle. Internal temperature served as a proxy for the system state. Because smooth trajectories can agree by chance, a four-parameter temperature model with a heating-cooling term was evaluated on held-out buckets and against 100 000 surrogate temperature courses with the same values and smoothness but randomised timing. For the nonlinear measures, the model predicted held-out buckets with a median skill of 0.48, better than a linear time trend, a time model with the same heating-cooling break and the surrogates ($p < 0.001$). The conventional indices reached

*Corresponding author. ORCID: 0009-0009-7121-0615.
Email address: jakob.eisenhauer.1533@student.lu.se (Jakob Eisenhauer)

0.12 and were not distinguishable from the surrogates ($p = 0.21$). The group difference exceeded that of the surrogates ($p < 0.001$). At equal temperature, the nonlinear measures differed between heating and cooling. Their skill was highest at 128–256 Hz (median held-out skill 0.70). The temperature model nearly matched a data-driven benchmark without temperature for the nonlinear measures (0.50), but not for the conventional indices (0.18). In-sample fits overstated predictive skill (median R^2 0.81 and 0.36), so held-out prediction against surrogate covariates provides a practical test for acoustic indicators in single experiments. Since the buckets replicate the measurement, not the process, replication across batches and cycles is needed.
Keywords: soil acoustics, ecoacoustic indices, permutation entropy, Lempel-Ziv complexity, composting, cross-validation, surrogate data

---

1. Introduction

Decomposition of organic matter links directly to carbon storage and nutrient availability in ecosystems. Litter carbon reaches soil organic matter through microbial processing, fragmentation and redistribution by soil fauna, and physical transfer (Cotrufo et al., 2015; Frouz, 2018). How a model represents the response of decomposition to temperature and moisture can substantially change simulated soil carbon stocks (Exbrayat et al., 2013), which motivates methods that follow changing substrate states continuously rather than only at the start and end of an experiment.

Most ways of tracking decomposition and related soil processes are destructive, labour intensive, or limited to occasional snapshots. Manual soil respiration surveys, for example, can miss short-term responses that

automated sampling detects (Savage and Davidson, 2003). Passive acoustic monitoring can record continuously with comparatively little effort (Gibb et al., 2019; Taylor et al., 2026). In soil, acoustic emissions have been linked to earthworm burrowing and root growth (Lacoste et al., 2018), acoustic complexity to animal richness and community composition (Maeder et al., 2022), and acoustic indices to abundance but not richness after restoration (Robinson et al., 2023) and to forest fire history and time of day (Metcalf et al., 2024a), while synthesised soundscapes showed that several indices track acoustic abundance but predict acoustic richness and evenness less reliably (Metcalf et al., 2024b). Across 34 studies, acoustic indices correlated only moderately and inconsistently with biodiversity (Alcocer et al., 2022). Acoustic-index guidance recommends matching measures to a defined ecological question (Bradfer-Lawrence et al., 2023). Here, the question is whether acoustic measures follow the changing thermal trajectory of a self-heating batch of decomposing material as a proxy for decomposition stages.

Measures of temporal organisation complement these indices. Permutation entropy (PE) summarises the diversity of ordinal patterns in a time series (Bandt and Pompe, 2002), and the LZ78 phrase count (LZC78) counts the distinct phrases into which Lempel-Ziv parsing divides a symbolic sequence (Ziv and Lempel, 1978). The two measures look at a series from two sides. PE is local, summarising the order of a few consecutive values, whereas LZC78 is global, accumulating new phrases over the whole sequence without restarting. Both have bioacoustic precedents. A PE representation tracked fish-chorus periods in noisy marine recordings more selectively than conventional indices

(Siddagangaiah et al., 2019), and Lempel-Ziv complexity, used as a similarity metric for animal vocal sequences, was robust to sample size in simulations (Kershenbaum and Garland, 2015). Weighted permutation entropy has also been used as an estimate of intrinsic predictability of ecological time series (Pennekamp et al., 2019). Whether such measures track the thermal phases of self-heating decomposition more consistently than conventional ecoacoustic indices has not been tested.

Self-heating decomposition, best known from composting, offers a controlled setting for this test. Organic material heats up while microbes mineralise simple compounds (Bernal et al., 2009). Once the most readily available resource is depleted, heat generation no longer offsets heat loss, and the internal temperature peaks and declines (Fan et al., 2021). The peak can serve as a proxy for a change in the character of decomposition, which in composting accompanies changes in microbial communities and material conditions (Meng et al., 2019). Temperature serves here as a reference for the state of the system, not as the quantity an acoustic indicator would replace. A thermometer records the heat balance, while sound may also register the phase at equal temperature and changes in activity that leave temperature unchanged, and in open soils there is no comparable self-heating signal.

Testing this in a single experiment has a statistical pitfall. Two smooth, trending series can be closely correlated without any connection (Granger and Newbold, 1974), so a high R^2 of a temperature model shows little on its own. Two safeguards were used. Models were judged by how well they predicted a bucket left out of the fit (Roberts et al., 2017; Sethi et al., 2023), and the temperature model was compared with surrogate temperature courses that

keep the values and smoothness of the real course but not its timing (Theiler et al., 1992; Schreiber and Schmitz, 1996). Together, they form a validation procedure that can be applied to any candidate acoustic indicator tested in a single experiment.

The study takes a system-level view, as advocated for soils as dynamic, emergent systems (Stroud et al., 2025). The decomposing batch is treated as one complex physical and biological system, and the acoustic measures are tested for whether they follow its emergent dynamics, not whether they identify individual organisms or processes. The study was designed as a proof of concept for the measures. Five buckets prepared from one vermicompost-hay batch were recorded repeatedly during a shared heating-cooling cycle, so that the material was held constant and four nonlinear measures could be compared with six conventional ecoacoustic indices across eight octave bands (consequences for inference: Section 3.6). Four questions were addressed, the first two with three designated primary tests and all other comparisons descriptive (Section 2.5). First, does a temperature model with a heating-cooling term predict held-out buckets better than time models and better than surrogate temperature courses? Second, does this differ between the nonlinear and the conventional measures? Third, how do predictive skill, temperature response and redundancy vary across measures and frequency bands? Fourth, do the buckets share structure that the temperature model does not capture?

2. Materials and methods

2.1. Experimental system and measurements

Five black, tapered polypropylene buckets (A – E) with a volume of 22.1 ± 0.6 L (Supplementary Methods) were filled to 20 ± 2 cm (about 15.5 ± 1.9 L) with reactivated vermicompost and hay at a wet-mass ratio of 2.00 ± 0.02 to 1. The hay originated from a low-fertility meadow with a low legume fraction, had been dried and stored for two years, and was cut to 10 ± 5 cm. The vermicompost had been reactivated seven days before monitoring. Buckets were covered with lightly stretched 50 µm low-density polyethylene film and kept indoors without direct sunlight or wind, standing on padding (Supplementary Methods).

Monitoring began on 27 June 2026 at 18:00 and covered 31 measurement occasions through 12 July 2026, normally twice daily in alternating afternoon (13:00) and evening (21:00) sessions. With one recorder, the buckets were recorded one after another, always in the order A to E and about 15 min apart. Of the 155 planned bucket-occasion recordings, three were not made because of a recorder malfunction and two were excluded because the recordings were damaged, probably by poor coupling between sensor and recorder. The 150 remaining recordings were analysed without imputation. At each occasion, all buckets were opened for about 1 min. Internal temperature was recorded at 14–15 cm depth with a TP101-type digital probe thermometer with a display resolution of 0.1 °C and a repeatability SD of 0.08 °C in a heat-bath test (Supplementary Methods). The same ALLSOUNDER ALISO recorder and piezoelectric soil probe (Elekon AG, Switzerland) were used throughout, with the probe inserted near the centre

of each bucket (±2 cm) at a depth of 10.5 ± 0.5 cm. Audio was stored as WAV at 48 kHz. Adult flies that emerged during the experiment were removed from the laboratory when detected. Measurement 1, a baseline recorded before the regular twice-daily schedule, entered all models as the first heating occasion. Temperature peaked at measurement 5 in all five buckets (Fig. 2, left).

Before-after mass and moisture measurements of every bucket gave two estimates of dry-mass loss, directly and from the retained metabolic water, with uncertainties propagated by a Monte Carlo simulation of 200 000 draws (Supplementary Methods).

2.2. Acoustic preprocessing

Octave bands were analysed separately because different sound sources tend to occupy different frequency ranges (Pijanowski et al., 2011; Aide et al., 2017). In forest soil, sounds attributed to the movement and feeding of nearby animals were reported at about 100 to 10 000 Hz (Maeder et al., 2022). The probe was inserted anew for each recording (11.5–15 min long). The first 1.0–4.5 min, which included the insertion and the initial settling of the probe, and the final 30 s were discarded, and the remaining 600 s were analysed. Signals were band-pass filtered into eight octave bands from 64–128 to 8192–16384 Hz (zero-phase Butterworth filters, order 6) and resampled to ten times the upper band edge, capped at 48 kHz. Frequencies below 64 Hz were excluded to reduce sensitivity to 50 Hz mains hum and other indoor anthrophony (traffic, building machinery), whose low frequencies buildings attenuate least (Berglund et al., 1996), and to the unspecified low-frequency response of the sensor. A further octave (16–32 kHz) would exceed the

Nyquist frequency at 48 kHz sampling.

Each 600 s excerpt was divided into 40 non-overlapping 15 s windows. For the nonlinear measures, each band signal was converted to a local root-mean-square (RMS) series. The RMS window and the delay τ (subsampling interval) of the symbolic analysis were not chosen band by band but follow one scaling law with the scale factor $\lambda = 3\,(f_{\max}/128\,\mathrm{Hz})^{-1/2}$, which falls by $\sqrt{2}$ per octave. The RMS window spans 5λ cycles of the lower band edge $f_{\min}$, and $\tau = \lambda f_s / f_{\max}$ samples (rounded, at least one). Both therefore shorten in a fixed proportion from the lowest to the highest octave (Supplementary Methods).

2.3. Acoustic measures

The nonlinear set comprised PE, LZC78, the relative sequence entropy (RSE_4) and the relative sequence redundancy (RSR). PE used ordinal patterns of order 4 (Bandt and Pompe, 2002). LZC78 was the number of phrases c in incremental LZ78 parsing of a symbol sequence over a 100-symbol alphabet (Ziv and Lempel, 1978). RSE_k and RSR estimate a variant of Shannon's redundancy: one minus the entropy rate of the symbol sequence divided by the single-symbol entropy H_1 (Shannon, 1948), which takes H_1 as reference instead of the maximum entropy. The ratio is 0 for a memoryless sequence and approaches 1 when each symbol is determined by its predecessors. The two differ only in the entropy-rate estimator: the block estimate H_k/k for RSE_k and the Lempel-Ziv estimate $c \log_2 c/N$ for RSR, which approaches the entropy rate for long sequences from stationary ergodic sources (Ziv and Lempel, 1978; Cover and Thomas, 1991). RSE_k

thus shares the local view of PE (words of k symbols), and RSR the global view of LZC78:

$$\mathrm{RSE}_k = \frac{kH_1 - H_k}{(k-1)H_1}, \qquad \mathrm{RSR} = 1 - \frac{c \log_2 c}{N H_1}, \tag{1}$$

where H_j is the base-2 entropy of length-j words and N the sequence length. RSE_4 ($k = 4$) used a 10-symbol alphabet and RSR the same sequence as LZC78 (derivation and rescaling: Supplementary Methods). Symbols were obtained with bucket-specific quantisers, fixed across all occasions within a band, with equal-width bins over the pooled 1st–99th percentile range. A level-invariant control with quantisers fitted per recording is described in the Supplementary Analyses (results: Section 3.3).

The conventional set comprised log band energy, the Acoustic Complexity Index (ACI; Pieretti et al., 2011), temporal and spectral entropy (Sueur et al., 2008b), spectral flatness as implemented in seewave (Sueur et al., 2008a, 2025), and a band-limited variant of the Acoustic Evenness Index (AEI; Villanueva-Rivera et al., 2011; Villanueva-Rivera and Pijanowski, 2018), all calculated from the band-limited signals as close to their original definitions as the octave scheme allowed (Supplementary Methods). Because these indices were designed for broadband spectra, they were also computed for one band from 64 to 16384 Hz with their standard parameters, as a reference.

The median of the 40 window values represented each bucket, occasion, measure and band. Values were standardised within each bucket and configuration with the mean and standard deviation over all available occasions, which removed between-bucket differences in level and spread, kept each bucket's trajectory and put all ten measures on a common scale.

Quantisers and standardisation used only the bucket's own data, so they did not link training and test buckets in the cross-validation.

2.4. Models

Each of the 80 measure-band configurations was modelled separately. For a configuration, y_{si} is the standardised value of bucket s at occasion i, t_i elapsed time in days, T_{si} the bucket's internal temperature, and C_i a cooling indicator that equals 1 after the peak of the mean temperature (measurements 6–31). The models were

$$\text{time-only:} \quad y_{si} = \alpha + \beta\, t_i + \varepsilon_{si}, \tag{2}$$

$$\text{temperature-only:} \quad y_{si} = \alpha + d\,(T_{si} - 30) + \varepsilon_{si}, \tag{3}$$

$$\text{L:} \quad y_{si} = \alpha + C_i\, b + (d + C_i\, e)\,(T_{si} - 30) + \varepsilon_{si}, \tag{4}$$

$$\text{L}_{\text{time}}\text{:} \quad y_{si} = \alpha + C_i\, b + (\beta + C_i\, e)\, t_i + \varepsilon_{si}. \tag{5}$$

Time-only and L_{time} are the competitors based on elapsed time. The primary model, L (for its piecewise-linear temperature response), lets the temperature response differ between heating and cooling, because after the peak the same temperature can correspond to a different process state (Section 1). Here, b is the offset of the cooling branch at 30 °C, d the temperature slope during heating and e its change after the peak. L_{time} has the same break and number of parameters as L but follows elapsed time within each phase, so it uses temperature only to place the break and tests whether L does more than separate the two phases.

A data-driven, nonparametric benchmark, model NP, tests whether the buckets share structure beyond what L captures. NP uses neither

temperature nor a functional form. It predicts a bucket by the mean trajectory $\bar{y}_j$ of the other buckets, smoothed over time with a Gaussian kernel,

$$\hat{y}_i = \frac{\sum_j w_{ij}\,\bar{y}_j}{\sum_j w_{ij}}, \qquad w_{ij} = \exp\!\left(-\frac{(t_i - t_j)^2}{2s^2}\right). \tag{6}$$

One bandwidth s, shared by all 80 configurations, was chosen from 0.4–4 days by leave-one-bucket-out cross-validation within the training buckets of each fold. The selected s was 0.75–1.0 days. Held-out skill of NP above that of L indicates shared variation that L misses.

2.5. Model evaluation

Each model was first fitted by ordinary least squares to the mean trajectory of the five buckets (with their mean temperature) and summarised by R^2. In leave-one-bucket-out cross-validation (Roberts et al., 2017), each model was then fitted to all values of four buckets, each with its own temperature, and predicted the fifth bucket from its own temperature, with the cooling indicator taken from the mean temperature of the training buckets. Skill was $1 - \mathrm{SSE}/\mathrm{SSE}_0$ on the held-out bucket, averaged over the five folds, where SSE_0 is the sum of squares of the standardised values. Skill above 0 means a better prediction than the bucket's own mean. Because each bucket was standardised with its own mean and standard deviation, skill refers to the shape of each bucket's trajectory, not its level.

Fitting the mean trajectory, rather than single buckets, is deliberate. The sound comes from discrete sources, such as individual animals, which are localised in space and move little during the 600 s of one recording, so a single probe partly records where a few sources happen to be. The target is the system that these organisms form, not single individuals, and averaging

over realisations of the same system, here the five buckets, suppresses this source-position noise. Whether the averaged trajectory reflects information common to the buckets is then tested by the held-out prediction, which is scored on the unaveraged values of a bucket not used in the fit.

The mean temperature course was then replaced by 100 000 surrogates generated with the iterative amplitude-adjusted Fourier transform (IAAFT; Schreiber and Schmitz, 1996), which keep its values exactly and its power spectrum approximately, and thus its smoothness, but randomise the timing of its rises and falls. For each surrogate, the temperature of every bucket was rebuilt as the surrogate course plus the real deviation of that bucket from the mean course at each occasion, so the differences between buckets were kept. The cooling phase was set to begin after the surrogate's own peak, and the models were refitted and cross-validated as above with the acoustic data unchanged. The statistic was the median held-out skill over a group of configurations, with $p = (1 + \#\{\text{surrogate} \geq \text{observed}\})/(1 + 100\,000)$ (Phipson and Smyth, 2010). Three tests, following the first two research questions, were designated as primary: model L in the nonlinear group, model L in the conventional group, and the difference in median skill of L between the two groups, tested against the same difference computed with each surrogate. All other p-values are descriptive. The same temperature surrogates also gave descriptive p-values for temperature-only and for $\mathrm{L}_{\mathrm{time}}$. Time itself was not surrogated. For $\mathrm{L}_{\mathrm{time}}$, only the break moved, to the peak of each surrogate. A further, conditional test used only the surrogates that placed the break exactly as the real course in every fold. They keep the phases of $\mathrm{L}_{\mathrm{time}}$ but change the temperature course within them. Because the

80 configurations share recordings, they are not independent tests, so each group is summarised by its median, not by its best configuration, since the highest of many values is optimistic (Forstmeier et al., 2017).

The uncertainty of the fits to the mean trajectory and of the coefficients of L was described by a two-level extension of the Bayesian bootstrap (Rubin, 1981) with 4 000 draws: Dirichlet weights over the 40 windows of each recording (weighted median) and over the five buckets (weighted mean trajectory), refitting the model in every draw. The 95% intervals are the 2.5th and 97.5th percentiles of the draws (Supplementary Methods). Agreement among buckets was described by the median Spearman correlation between the time courses of all ten bucket pairs. Redundancy was described by Spearman correlations between all 80 configurations, with $|\rho| \geq 0.95$ flagged descriptively. It was also described by cross-prediction between groups, in which ridge regression predicted every configuration of one group from all configurations of the other in held-out buckets (Supplementary Methods). In a parameter sensitivity experiment, held-out skill was recomputed for 18 preprocessing settings and for centring within buckets without scaling (Supplementary Methods and Table S2). Residual diagnostics and signal-level surrogates of the recordings are reported in the Supplementary Analyses, as are nine further checks of the temperature input, the heating phase, added covariates, the highest band and the absolute level.

All analyses used Python with NumPy (Harris et al., 2020), pandas (McKinney, 2010), SciPy (Virtanen et al., 2020), SoundFile (Bechtold, 2026), Numba (Lam et al., 2015) and Matplotlib (Hunter, 2007). Random seeds are fixed. The analysis and figure code was written and restructured with the

assistance of Claude Sonnet 5.5 and Claude Opus 5.5 (Anthropic) under the author's direction. All results and figures are produced by the released code. Data and code are archived on Zenodo (Eisenhauer, 2026b,a).

3. Results and discussion

3.1. Fit, prediction of held-out buckets and comparison of the measure groups

Internal temperature rose from 28 to 39 °C within two days, peaked at measurement 5 and declined to 26 °C, almost identically in all five buckets (Fig. 2, left). The batch thus self-heated within the mesophilic range and remained below the temperatures of active composting, with an optimum of 40–65 °C and above 55 °C for sanitisation (Bernal et al., 2009). Over the experiment, the dry mass of the material decreased by 23.6% of its initial value (95% Monte Carlo interval 20.8–26.3%) by the direct estimate and by 20.1% (14.1–26.3%) by the retained-water estimate (Supplementary Methods and Table S4). The heating-cooling cycle was thus accompanied by a large loss of dry matter, whose share of microbial and faunal activity was not resolved. Fig. 1 shows model L for RSR in three octave bands. At 128–256 Hz, RSR was highest at the start, fell steeply during the first three days and levelled off after about day 6. At 1024–2048 Hz, it reached its minimum about one day after the temperature peak and then rose, and at 4096–8192 Hz the minimum coincided with the peak. L, which uses only the temperature course and the heating-cooling phase, followed all three shapes, which a linear time trend cannot. Supplementary Fig. S1 shows all 80 configurations with the time-only fit.

Fitted to the mean trajectories, the models explained much of the variation,

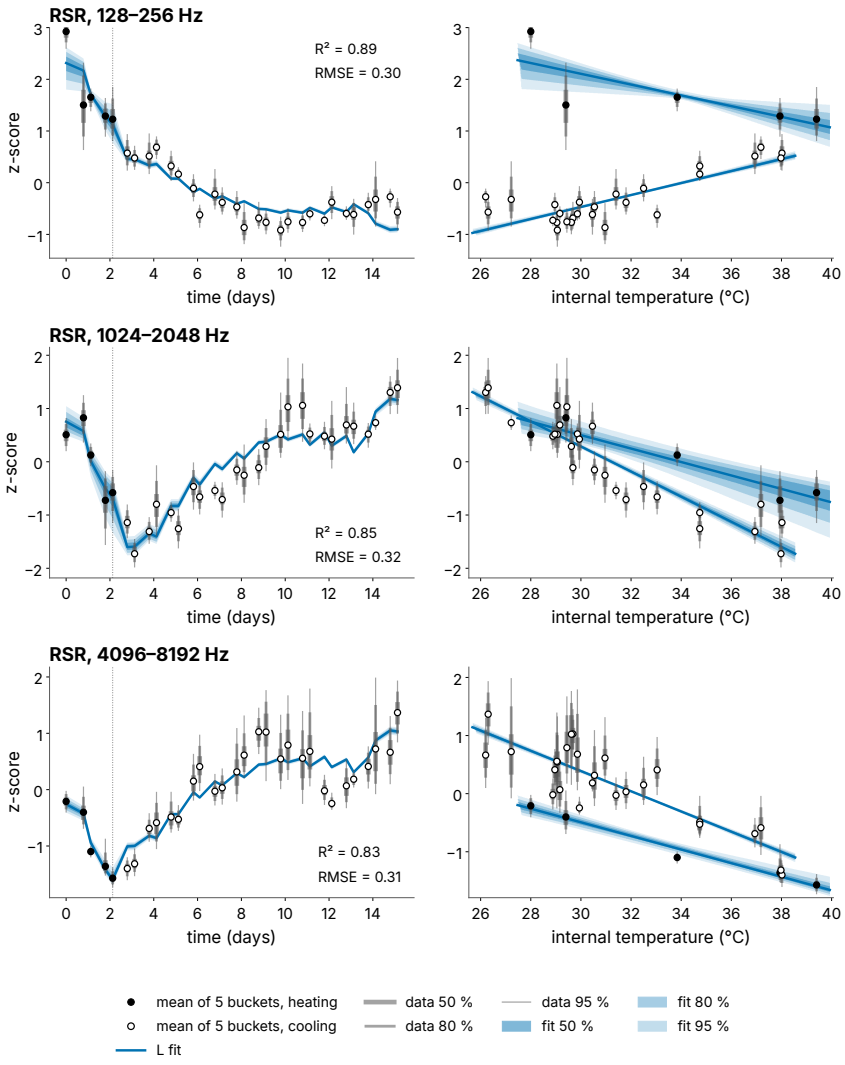


Figure 1: Fit of model L to the mean trajectory of RSR over time (left) and temperature (right) at 128–256, 1024–2048 and 4096–8192 Hz. Points: mean of buckets A–E, filled during heating and open during cooling (after the temperature peak, dotted line); grey bars: 50, 80 and 95% intervals of the mean trajectory over the Bayesian bootstrap draws; blue line: L fitted to the observed data; blue ribbons: 50, 80 and 95% intervals of the refitted L. In the temperature panels, the two lines are the heating and the cooling branch of L. The heating branch has only five measurements, hence its wider intervals. R^2 and RMSE refer to the fit to the mean trajectory.

far more for the nonlinear measures (median R^2 of L 0.81) than for the conventional indices (0.36; Table 1). For held-out buckets, the median skill for the nonlinear measures was 0.33 for time-only, 0.30 for temperature-only and 0.48 for L. Temperature as a single linear term therefore added nothing to a time trend, while L, which lets the response differ between heating and cooling, predicted better than both time-only and temperature-only in 28 of 32 nonlinear configurations. The time model with the same break, L_{time}, reached 0.40. L predicted better in 26 of 32 nonlinear configurations and for every held-out bucket (median gain 0.03–0.05 per bucket), so separating the two phases explains only part of the advantage of L. With the mean temperature of the training buckets in place of each bucket's own temperature, the skill of L changed by a median of 0.004, so the information lies in the shared temperature course, not in the small differences between buckets (median 0.16 °C). Still, within occasions, where elapsed time was the same for all buckets, the small temperature differences between buckets were followed by acoustic differences of the size predicted by L. Over all 80 configurations, the ratio of observed to predicted differences was 1.03 ($p = 0.015$, descriptive; Supplementary Analyses). Adding a linear time term to L changed the median held-out skill by at most 0.02 (nonlinear 0.49, conventional 0.15). Neither an afternoon/evening nor a mains-hum term improved the nonlinear median (-0.001 and -0.006; Supplementary Table S6).

For the conventional indices, held-out skill was low for all models (0.07–0.12). L improved on time-only in 42 of 48 conventional configurations, but the median gain was small (from 0.07 to 0.12). Among the conventional indices,

Table 1: Model comparison, medians over the configurations of each measure group. Time-only and temperature-only have two parameters, L_{time} and L four. R^2: fit to the mean trajectory of buckets A–E. Skill: prediction of held-out buckets ($1 - SSE/SSE_0$, mean of five folds). p: share of 100 000 IAAFT temperature surrogates whose median skill reached the observed one (for L_{time}, the surrogates move only its break); bold: primary tests (the third, the difference between the groups, is given in Section 3.2). NP: data-driven benchmark without temperature (about 8.8 effective degrees of freedom; Section 3.5).

	Nonlinear (32)			Conventional (48)		
Model	R^2	skill	p	R^2	skill	p
time-only	0.545	0.329	–	0.203	0.067	–
temperature-only	0.513	0.300	0.020	0.204	0.071	0.094
L_{time}	0.685	0.397	0.162	0.310	0.084	0.678
L	0.810	0.485	**0.00003**	0.360	0.124	**0.206**
NP	0.887	0.500	–	0.687	0.178	–

only log band energy predicted well (median skill of L 0.40). In the bands from 64 to 512 Hz it mostly shares its information with LZC78 (Section 3.4). Computed broadband with their standard parameters, the conventional indices predicted held-out buckets better than in single octaves (median skill of L 0.22), but still not distinguishably from the surrogates ($p = 0.11$) and well below the nonlinear measures (Supplementary Table S3). The advantage of L over time-only in both groups, and over L_{time} in the nonlinear group, held in all 19 settings of the sensitivity analysis, including centring without scaling. Across these settings, the median nonlinear skill of L ranged from 0.40 to 0.50 (Supplementary Table S2 and Figs. S5 and S6).

The five buckets also followed more similar time courses under the nonlinear measures, with a median Spearman correlation between bucket pairs of 0.57 against 0.33. Within the nonlinear group, the median held-out skill of L was 0.53 for RSE_4 and RSR, 0.50 for LZC78 and 0.31 for PE. Among the conventional indices, only log band energy (0.40) reached this range. Grouped by octave band or by measure, the nonlinear categories occupied the upper ranks for all four models, with log band energy and the conventional 256–1024 Hz bands as the only overlap. L was above time-only and temperature-only in most categories (Supplementary Fig. S3).

With signal-level IAAFT surrogates of the recordings, distinct from the temperature surrogates, observed and surrogate values differed in 28 of 32 nonlinear configurations (median absolute difference 0.37 standard deviations), whereas synthetic linear Gaussian signals produced no systematic differences ($p \geq 0.52$ for all four measures; Supplementary Analyses). The recorded sound therefore contains temporal structure

that a stationary linear process with the same spectrum and amplitude distribution does not reproduce. Possible sources are nonlinear dynamics and non-stationarity within the 15 s windows.

3.2. Temperature surrogates

With the surrogates (Fig. 2, left) in place of the real temperature, L reached a median held-out skill of 0.29 in the nonlinear group (95th percentile 0.41). The real course, with 0.48, predicted held-out buckets better than 99 998 of the 100 000 surrogates ($p = 0.00003$; Fig. 2, right). The distribution is bimodal because surrogates that peak early reach about the skill of the time-only model (Supplementary Results). The timing of the real temperature course is therefore associated with the acoustic trajectories of this batch more closely than smooth curves with the same values. For the conventional group, L reached a median skill of 0.12 and did not exceed the surrogates (surrogate median 0.09, $p = 0.21$).

Because each surrogate also moves the break of L, two further comparisons separated the timing of the break from the temperature course within the phases. L_{time} reached a median skill of 0.40 and did not exceed the surrogates (surrogate median 0.37, $p = 0.16$, descriptive). In the conditional test, restricted to the 3 298 surrogates that placed the break as the real course did in every fold, L reached a median skill of 0.28 (95th percentile 0.44), against 0.48 with the real course ($p = 0.0006$), even though these surrogates resembled the real course more closely than the others (median correlation 0.65). Within the same two phases, the real temperature course predicted the buckets better than temperature-like courses, so temperature carried

information within each phase, not only through the position of the break.

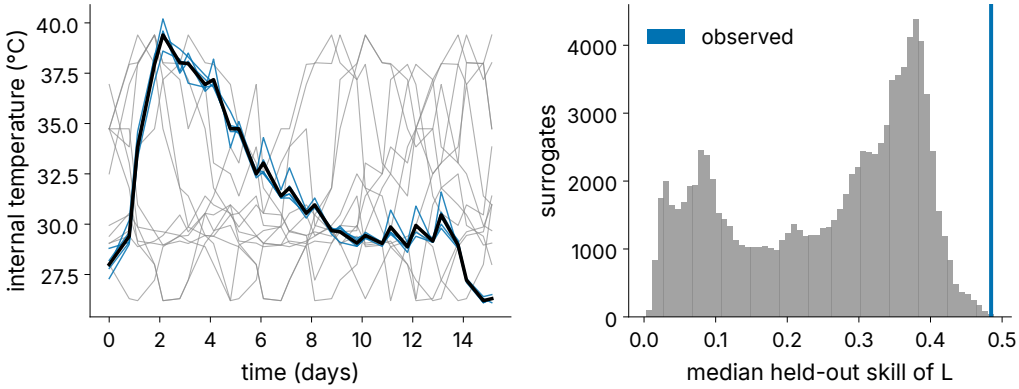


Figure 2: Temperature-surrogate test. Left: internal temperature of buckets A–E (blue), their mean (black) and 12 of the 100 000 IAAFT surrogates of the mean (grey), which keep its values exactly and its power spectrum approximately but not the timing of its rises and falls. Right: median held-out skill of model L over the 32 nonlinear configurations with each surrogate (grey histogram) and with the real temperature (blue line).

The difference between the groups, the third test, also depended on the real course. The median skill of L was 0.36 higher for the nonlinear than for the conventional group. With the surrogates, this difference was 0.20 in the median and reached 0.36 in only 22 of 100 000 cases ($p = 0.00023$). Part of the nonlinear advantage thus reflects smoother, more predictable trajectories in general, and a further part depends on the timing of the real temperature course.

3.3. The heating-cooling terms

In the fit to the mean trajectory, the 95% Bayesian-bootstrap interval of the cooling offset b excluded zero in 28 of 32 nonlinear and 39 of 48 conventional configurations; for the slope change e, in 22 of 32 and 38 of 48

(Supplementary Fig. S7). In temperature space, L consists of one line per phase, and the same temperature corresponded to different acoustic values during heating and cooling (Fig. 1), a hysteresis-like pattern. At the middle of the temperature range covered by both phases (33 °C), the cooling branch of RSR lay 1.9 standard deviations below the heating branch at 128–256 Hz (95% Bayesian-bootstrap interval 1.8–2.0), 0.5 below it at 1–2 kHz (0.2–0.9) and 0.7 above it at 4–8 kHz (0.6–0.8). The 95% interval of this difference between the branches, $b + e\,(T - 30)$, excluded zero in 28 of 32 nonlinear configurations. In 8 of the 32 (4 of these 28) the branches crossed within this range, so there they differed mainly in slope rather than in level. For RSR at 1–2 kHz, for example, the cooling branch fell almost twice as steeply. The difference between the branches also speaks against a purely instrumental explanation. The sensitivity and self-noise of a piezoelectric sensor change with its temperature, but such an effect depends on the current temperature only and would give the same values at the same temperature in both phases. Moreover, sensor self-noise would not produce the structure that the signal-level surrogates showed (Section 3.1). Fig. 1 also shows where L falls short. The mean trajectory of RSR at 1–2 kHz lies below the fit around days 5–9 and above it around days 10–13, so the residuals remain partly structured (Section 3.5).

The heating branch of L has only five occasions (measurements 1–5), while the 26 cooling occasions dominate the overall skill. Scored separately, the nonlinear median skill of L was 0.70 on heating and 0.42 on cooling occasions (Supplementary Table S5). When one heating occasion at a time was left out, the cooling offset b kept its sign in 30 of 32 nonlinear configurations, the

slope difference e in 27 and the difference between the branches at 33 °C in 30. The heating slope d was the least stable (26 of 32) but does not enter the difference between the branches, $b + e\,(T - 30)$, and thus says nothing about the separation of heating and cooling.

Moisture, compaction and organic matter change the attenuation of sound in soil (Oelze et al., 2002; Taylor et al., 2026). Within one octave band, such changes are expected to act mainly on the absolute level. The movement and feeding of fauna, by contrast, produce discrete and partly rhythmic sounds (Lacoste et al., 2018; Maeder et al., 2022) that change not only the level but also the temporal pattern. As a level-invariant control, the quantiser of LZC78, RSE_4 and RSR was fitted for every recording separately, which removed the absolute level from these measures (Supplementary Analyses). PE does not depend on the level. Because the level also carries faunal information, smaller effects were expected. The heating-cooling terms persisted at a smaller size. The 95% interval of b excluded zero in 26 of 32 nonlinear configurations (28 in the main analysis) and that of e in 24 (22), and the median difference between the branches at 33 °C fell from 0.71 to 0.40 standard deviations. Held-out skill dropped for both L (median 0.17 instead of 0.48) and the time-only model (0.09 instead of 0.33), but L still predicted better than time-only in 29 of 32 configurations (30). Hence the difference between heating and cooling cannot be explained by changes in attenuation alone. Whether its smaller size reflects a share of attenuation or the faunal information removed with the level cannot be separated here.

3.4. Frequency dependence and redundancy

Fig. 3 shows the best and the median configuration of each group in every octave band. The median nonlinear configuration predicted held-out buckets better than the median conventional one in every band except 512–1024 Hz (0.28 against 0.31). The nonlinear group performed best at 128–256 Hz (median R^2 of L 0.88, median held-out skill 0.70), was lowest at 512–1024 Hz, remained near 0.30 up to 4096 Hz and reached 0.50 at 4096–8192 Hz. The median conventional configuration was best at 512–1024 Hz, with less than half the held-out skill of the best nonlinear band (0.31; R^2 per band: Supplementary Fig. S4). The in-sample R^2 overstated held-out skill relatively more for the conventional indices in seven of eight bands (all except 512–1024 Hz).

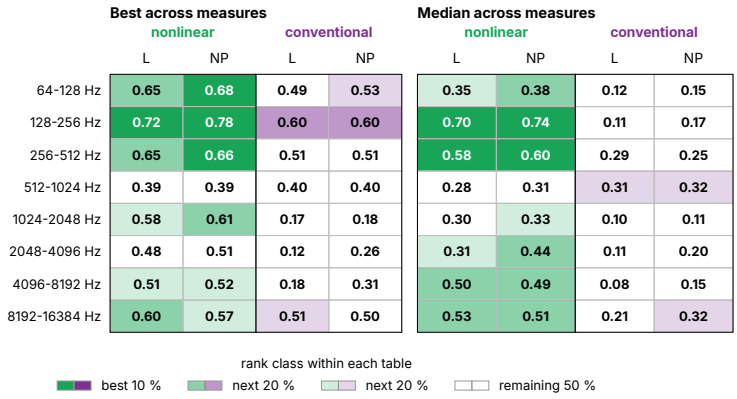


Figure 3: Held-out skill per octave band of L and NP, for the best (left) and the median configuration (right) of each group (nonlinear: 4 measures per band, conventional: 6). Hue: measure group (nonlinear green, conventional purple); shading ranks the 32 cells within each table. Values per configuration: Supplementary Fig. S2.

Some coefficients of L also shifted with frequency (Fig. 4; all measures:

Supplementary Fig. S7). For RSR and RSE_4, the cooling offset b changed sign near 1 kHz (for RSR in Fig. 1). For LZC78 it decreased steadily from about +2 below 512 Hz to near zero at 4096–8192 Hz. Other coefficients, such as the heating slope d of RSR (negative in seven of eight bands), kept their sign across most bands. The sign changes could reflect different low- and high-frequency responses to the transition, for example through different sound sources or transmission paths, that partly cancel around 1 kHz, but the data do not test this.

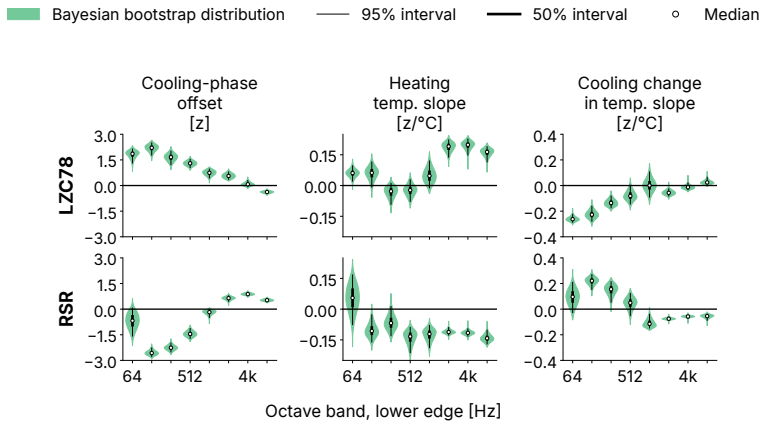


Figure 4: Coefficients of L by octave band for LZC78 and RSR: cooling offset b, heating slope d and slope change after the peak e (Eq. 4). Violins: distribution over the Bayesian bootstrap draws; thin and thick bars: 95 and 50% intervals; white dot: median. All measures: Supplementary Fig. S7.

Strong redundancy ($|\rho| \geq 0.95$) was confined to a few pairs of measures in the same band (Fig. 5; all pairs: Supplementary Results). Spectral entropy and spectral flatness exceeded it in all eight bands, as expected for nearly flat spectra (Supplementary Results). Between the groups, LZC78 and log band energy exceeded it in the three bands from 64 to 512 Hz and at

8192–16384 Hz, so the good prediction of log band energy in the low bands largely repeats that of LZC78. RSE_4 and RSR, two estimators of the same quantity, were correlated at 0.80–0.98, but in the lowest band RSE_4 predicted held-out buckets better (0.48 against 0.23). Between two frequency bands, only RSR at 2048–4096 and 4096–8192 Hz reached the threshold ($\rho = 0.95$). Taken jointly, however, the groups shared most of their variation. The conventional indices predicted the nonlinear measures of held-out buckets with a median skill of 0.85, and the nonlinear measures predicted the conventional indices with 0.65 (Supplementary Results). The comparison is not symmetric, because the conventional set has more predictors (48 against 32) and conventional configurations that carry mostly noise are harder to predict as targets.

3.5. Shared structure beyond temperature

The data-driven model NP tested whether the structure that L leaves out is shared by the buckets and thus could be predicted. For the nonlinear measures, NP predicted held-out buckets about as well as L (median skill 0.50 against 0.48; Fig. 3 and Supplementary Fig. S3), so NP gave little evidence of shared structure beyond L. For the conventional indices, NP was better (0.18 against 0.12). The gain was uneven. NP exceeded L by more than 0.10 in 16 of 80 configurations, 13 of them conventional, and fell below it by more than 0.05 in only two. Gains concentrated above 2048 Hz and at 64–128 Hz and in PE, ACI and temporal entropy, where NP reached median skills of 0.42, 0.23 and 0.27 against 0.31, 0.16 and 0.16 for L. For LZC78, RSE_4 and RSR, L was as good or better. In the clearest case, PE at 4096–8192 Hz, all five buckets dipped around days 8–10, with no counterpart in the temperature

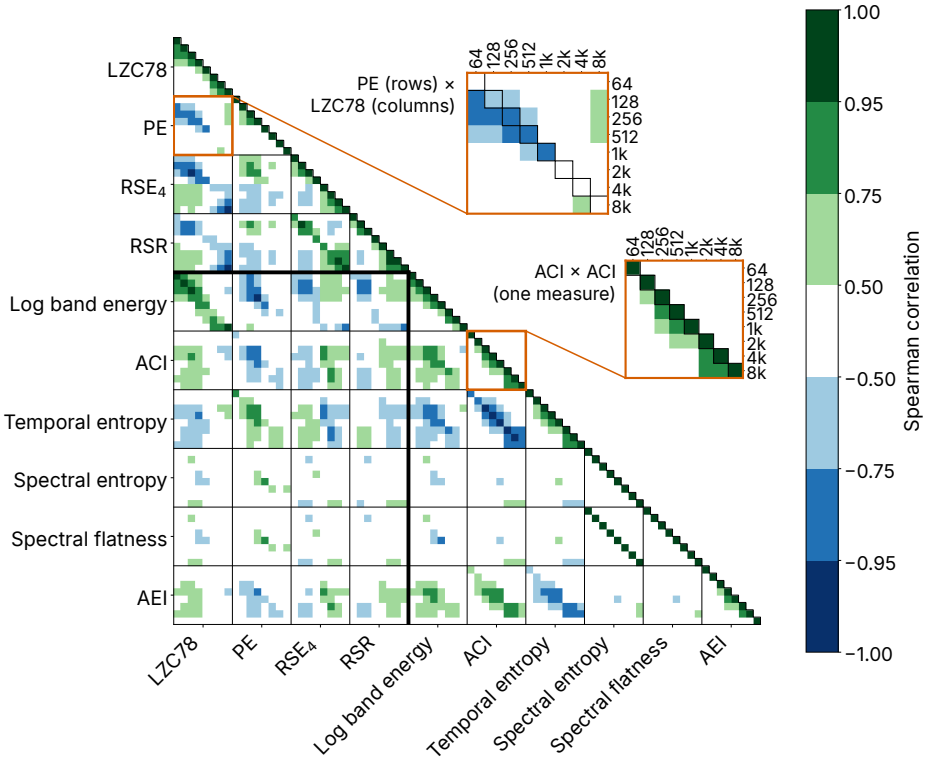


Figure 5: Correlation structure and redundancy: Spearman correlations among all 80 measure-band trajectories (within-bucket standardised bucket-occasion values), lower triangle only. Each block is the 8×8 band-by-band matrix for one pair of measures. Thick lines separate the nonlinear (top left) from the conventional measures (bottom right). Orange: two blocks enlarged, with bands labelled by their lower edge and the same-band cells outlined. Colour classes: $|\rho| \geq 0.95$ (the descriptive redundancy threshold), 0.75–0.95 and 0.50–0.75, green for positive and blue for negative correlations; white: $|\rho| < 0.50$.

course. NP followed the dip and predicted held-out buckets with a skill of 0.46, against 0.26 for L (Fig. 6).

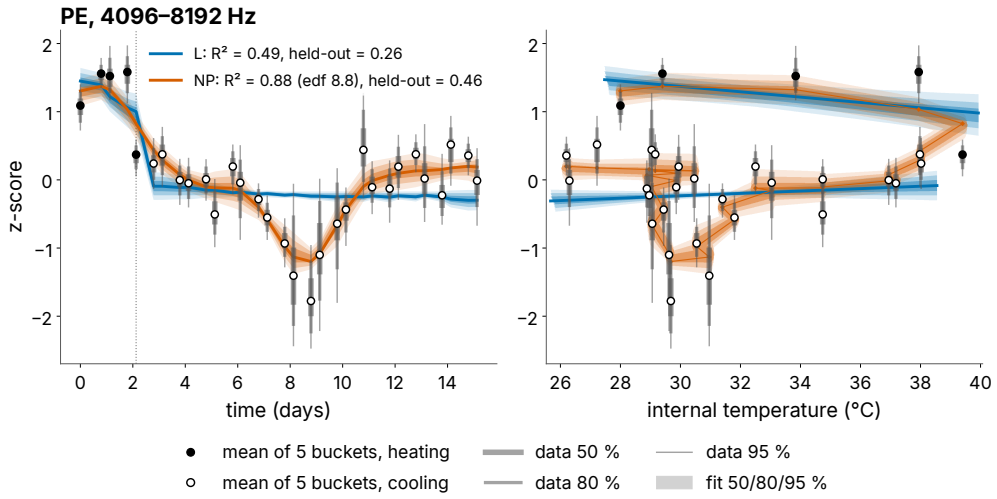


Figure 6: PE at 4096–8192 Hz over time (left) and temperature (right), fitted by L (blue) and by the data-driven shared curve NP (orange), which in the temperature panel is drawn as its path in time order. Black points: mean of buckets A–E; grey bars as in Fig. 1; ribbons: 50, 80 and 95% intervals of the refitted models over the Bayesian bootstrap draws. R^2: fit to the mean trajectory (NP with 8.8 effective degrees of freedom); held-out skill: leave-one-bucket-out.

Faunal development, for example the temperature-dependent stages of fly larvae (Powsner, 1935; Grassberger and Reiter, 2001), may contribute to such shared variation. The dip fell into the period in which adult *Drosophila* and blowflies (*Lucilia* sp.) appeared (days 7–13), when at least part of their larvae had probably stopped feeding and pupated. The fly sightings were opportunistic observations from the protocol notes (Supplementary Methods). Faunal density and positions were not monitored, so no mechanism is attributed and verification requires visual or destructive

designs. The measures showed this variation to different degrees, PE more than LZC78, RSE_4 and RSR. With the absolute level removed (Section 3.3), the residuals of L in these three measures followed those of PE at 1–8 kHz ($|r| = 0.65$–0.89; Supplementary Table S10). RSR at 4096–8192 Hz also showed the dip around days 8–10 (Supplementary Fig. S9). Whether combinations of measures can separate the thermal response from other shared dynamics remains to be tested. The comparison is exploratory. NP is more flexible than L, so it is a benchmark for shared structure rather than a competing explanation, and no surrogate test was applied to it.

3.6. Limitations

The experiment comprised one heating-cooling cycle, so temperature and elapsed time changed together. Only further cycles with different temperature courses can fully separate them. A comparison within occasions, where elapsed time was the same for all buckets, is consistent with a temperature effect beyond the shared time course (Section 3.1) but is based on a narrow temperature contrast.

By design, the five buckets came from one batch, one cycle and one indoor environment. Within this batch, they are replicates ($n = 5$). Each bucket decomposed and was recorded separately. However, they share their initial conditions (material, mixing ratio, starting moisture and biota) and part of their boundary conditions (room temperature, background noise, air pressure, recording schedule), so as a sample of decomposition systems in general they are pseudoreplicates of one system ($n = 1$; Hurlbert, 1984). This suits a proof of concept for the measures, but held-out skill and surrogate

p-values refer to prediction within this system, not to transfer to other batches, substrates, cycles or thermophilic conditions. Because the buckets followed almost the same temperature course, held-out skill measures how reproducibly the acoustic response appeared across buckets, not how well it generalises to other temperature courses.

The internal temperature is a proxy for decomposition stages, not a measurement of decomposition itself. Biological activity (such as the succession of microbes (Meng et al., 2019) and fauna), moisture (Richard et al., 2002), oxygen and sound transmission (Oelze et al., 2002) were not resolved through time, so the heating-cooling terms are not attributed to a specific mechanism. The heating branch of L is based on few occasions (Section 3.3). The temperature response of the sensor was not calibrated, although the difference between the branches argues against it as the main driver. Changes in coupling or sound transmission with moisture and settling of the material (Oelze et al., 2002; Taylor et al., 2026) could produce a similar difference. The measures would then still indicate the state of the material, but not necessarily biological activity.

Of the 32 nonlinear measure-band pairs, 12 reached $|\rho| \geq 0.85$ with log band energy (Supplementary Results). Band energy may limit the interpretation in two ways, depending on the frequency range. Below 2048 Hz, it rose by 4–10 dB between the first and last three occasions, which may indicate a contribution of changed attenuation to the signal. In the level-invariant control, the heating-cooling terms persisted at a smaller size (Section 3.3). Between 2048 and 8192 Hz, the net change was less than 1 dB. At 8192–16384 Hz, band energy varied by only about 1 dB, so

a small temperature response of the sensor, amplified by within-bucket standardisation and the fixed quantiser, could affect the results of correlated measures in this band. The conclusions do not rest on this band (results without this band: Supplementary Table S8).

The residuals of L remained autocorrelated (Supplementary Analyses), and the Bayesian bootstrap reweights only five buckets and treats the windows of a recording as exchangeable, so coefficient intervals are approximate. The held-out skill and the surrogate test do not assume independent errors. RSE_4 and RSR combine standard entropy-rate estimators with a standard reference, but their finite-sample behaviour at the window lengths and alphabets used here was examined only in the sensitivity analysis, not validated independently.

4. Conclusion

The nonlinear complexity measures followed the heating-cooling cycle of the monitored batch. A temperature model with a heating-cooling term predicted held-out buckets better than models based on elapsed time and better than temperature-like surrogates, including surrogates with the real break. The measures differed between heating and cooling at equal temperature. The conventional indices did not separate from the surrogates. Skill varied with frequency. Strong pairwise redundancy was limited to a few measure pairs within a band, although jointly the two groups shared most of their variation within a recording. Some measures also showed shared variation over days that temperature does not explain and whose origin remains open.

Combining held-out buckets with surrogate covariates separates agreement with the reference course from agreement with any smooth trend, which in-sample R^2 alone cannot. Because it requires only one experiment, this test can screen candidate acoustic indicators before replicated studies are designed.

The results hold within one batch and cycle and are a first indication. Their transferability to other batches, substrates and cycles is unknown. The next steps are replication with independent batches and a second cycle with a different temperature course, ideally with direct measurements of respiration, moisture, oxygen and biological activity, and then application in open soils, where several inexpensive probes within one system can take the place of the buckets.

Data and code availability

The 150 analysed recordings and the measurement protocol are archived on Zenodo (Eisenhauer, 2026b), under a CC BY 4.0 licence (https://doi.org/10.5281/zenodo.23891122). The analysis code, which reproduces all results, tables and figures, is archived on Zenodo (Eisenhauer, 2026a), under an MIT licence (https://doi.org/10.5281/zenodo.23959730).

Funding

This research was funded by the author and received no external funding.

CRediT authorship contribution statement

Jakob Eisenhauer: Conceptualization, Methodology, Software, Validation, Formal analysis, Investigation, Resources, Data curation, Writing – original draft, Writing – review & editing, Visualization, Project administration.

Declaration of competing interest

The author declares no competing financial interests or personal relationships that could have appeared to influence the work reported in this paper.

Declaration of generative AI and AI-assisted technologies in the writing process

During the preparation of this work the author used Claude Sonnet 5.5 and Claude Opus 5.5 (Anthropic), iteratively and under the author's direction. *Coding:* setting up, editing and restructuring the codebase. *Writing:* language editing and rephrasing at the level of individual sentences. *Review:* drafts of the manuscript were reviewed by AI, and its feedback prompted revisions. The author reviewed and edited all content as needed and takes full responsibility for the content of the publication.

References

Aide, T.M., Hernández-Serna, A., Campos-Cerqueira, M., Acevedo-Charry, O., Deichmann, J.L., 2017. Species richness (of insects) drives the use of acoustic space in the tropics. Remote Sensing 9, 1096. doi:10.3390/rs9111096.

Alcocer, I., Lima, H., Sugai, L.S.M., Llusia, D., 2022. Acoustic indices as proxies for biodiversity: a meta-analysis. Biological Reviews 97, 2209–2236. doi:10.1111/brv.12890.

Bandt, C., Pompe, B., 2002. Permutation entropy: a natural complexity measure for time series. Physical Review Letters 88, 174102. doi:10.1103/PhysRevLett.88.174102.

Bechtold, B., 2026. python-soundfile: an audio library based on libsndfile, CFFI and NumPy, version 0.14.0. https://github.com/bastibe/python-soundfile.

Berglund, B., Hassmén, P., Job, R.F.S., 1996. Sources and effects of low-frequency noise. The Journal of the Acoustical Society of America 99, 2985–3002. doi:10.1121/1.414863.

Bernal, M.P., Alburquerque, J.A., Moral, R., 2009. Composting of animal manures and chemical criteria for compost maturity assessment. A review. Bioresource Technology 100, 5444–5453. doi:10.1016/j.biortech.2008.11.027.

Bradfer-Lawrence, T., Desjonqueres, C., Eldridge, A., Johnston, A., Metcalf, O., 2023. Using acoustic indices in ecology: guidance on study design, analyses and interpretation. Methods in Ecology and Evolution 14, 2192–2204. doi:10.1111/2041-210X.14194.

Cotrufo, M.F., Soong, J.L., Horton, A.J., Campbell, E.E., Haddix, M.L., Wall, D.H., Parton, W.J., 2015. Formation of soil organic matter via

biochemical and physical pathways of litter mass loss. Nature Geoscience 8, 776–779. doi:10.1038/ngeo2520.

Cover, T.M., Thomas, J.A., 1991. Elements of Information Theory. Wiley, New York. doi:10.1002/0471200611.

Eisenhauer, J., 2026a. Hearing the heat: analysis code, version 1.2.0. Zenodo. https://doi.org/10.5281/zenodo.23959730.

Eisenhauer, J., 2026b. Hearing the heat: soil probe recordings of rapid organic decomposition (150 x 10 min), version 1.0.0. Zenodo. https://doi.org/10.5281/zenodo.23891122.

Exbrayat, J.F., Pitman, A.J., Zhang, Q., Abramowitz, G., Wang, Y.P., 2013. Examining soil carbon uncertainty in a global model: response of microbial decomposition to temperature, moisture and nutrient limitation. Biogeosciences 10, 7095–7108. doi:10.5194/bg-10-7095-2013.

Fan, S., Li, A., ter Heijne, A., Buisman, C.J.N., Chen, W.S., 2021. Heat potential, generation, recovery and utilization from composting: A review. Resources, Conservation and Recycling 175, 105850. doi:10.1016/j.resconrec.2021.105850.

Forstmeier, W., Wagenmakers, E.J., Parker, T.H., 2017. Detecting and avoiding likely false-positive findings – a practical guide. Biological Reviews 92, 1941–1968. doi:10.1111/brv.12315.

Frouz, J., 2018. Effects of soil macro- and mesofauna on litter decomposition and soil organic matter stabilization. Geoderma 332, 161–172. doi:10.1016/j.geoderma.2017.08.039.

Gibb, R., Browning, E., Glover-Kapfer, P., Jones, K.E., 2019. Emerging opportunities and challenges for passive acoustics in ecological assessment and monitoring. Methods in Ecology and Evolution 10, 169–185. doi:10.1111/2041-210X.13101.

Granger, C.W.J., Newbold, P., 1974. Spurious regressions in econometrics. Journal of Econometrics 2, 111–120. doi:10.1016/0304-4076(74)90034-7.

Grassberger, M., Reiter, C., 2001. Effect of temperature on *Lucilia sericata* (Diptera: Calliphoridae) development with special reference to the isomegalen- and isomorphen-diagram. Forensic Science International 120, 32–36. doi:10.1016/S0379-0738(01)00413-3.

Harris, C.R., Millman, K.J., van der Walt, S.J., Gommers, R., Virtanen, P., Cournapeau, D., Wieser, E., Taylor, J., Berg, S., Smith, N.J., Kern, R., Picus, M., Hoyer, S., van Kerkwijk, M.H., Brett, M., Haldane, A., del Río, J.F., Wiebe, M., Peterson, P., Gérard-Marchant, P., Sheppard, K., Reddy, T., Weckesser, W., Abbasi, H., Gohlke, C., Oliphant, T.E., 2020. Array programming with NumPy. Nature 585, 357–362. doi:10.1038/s41586-020-2649-2.

Hunter, J.D., 2007. Matplotlib: a 2D graphics environment. Computing in Science & Engineering 9, 90–95. doi:10.1109/MCSE.2007.55.

Hurlbert, S.H., 1984. Pseudoreplication and the design of ecological field experiments. Ecological Monographs 54, 187–211. doi:10.2307/1942661.

Kershenbaum, A., Garland, E.C., 2015. Quantifying similarity in animal vocal sequences: which metric performs best? Methods in Ecology and Evolution 6, 1452–1461. doi:10.1111/2041-210X.12433.

Lacoste, M., Ruiz, S., Or, D., 2018. Listening to earthworms burrowing and roots growing – acoustic signatures of soil biological activity. Scientific Reports 8, 10236. doi:10.1038/s41598-018-28582-9.

Lam, S.K., Pitrou, A., Seibert, S., 2015. Numba: a LLVM-based Python JIT compiler, in: Proceedings of the Second Workshop on the LLVM Compiler Infrastructure in HPC, pp. 1–6. doi:10.1145/2833157.2833162.

Maeder, M., Guo, X., Neff, F., Schneider Mathis, D., Gossner, M.M., 2022. Temporal and spatial dynamics in soil acoustics and their relation to soil animal diversity. PLOS ONE 17, e0263618. doi:10.1371/journal.pone.0263618.

McKinney, W., 2010. Data structures for statistical computing in Python, in: Proceedings of the 9th Python in Science Conference, pp. 56–61. doi:10.25080/Majora-92bf1922-00a.

Meng, Q., Yang, W., Men, M., Bello, A., Xu, X., Xu, B., Deng, L., Jiang, X., Sheng, S., Wu, X., Han, Y., Zhu, H., 2019. Microbial community succession and response to environmental variables during cow manure and corn straw composting. Frontiers in Microbiology 10, 529. doi:10.3389/fmicb.2019.00529.

Metcalf, O.C., Baccaro, F., Barlow, J., Berenguer, E., Bradfer-Lawrence, T., Rossi, L.C., do Vale, É.M., Lees, A.C., 2024a. Listening to tropical forest

soils. Ecological Indicators 158, 111566. doi:10.1016/j.ecolind.2024.111566.

Metcalf, O.C., Nunes, C.A., Abrahams, C., Baccaro, F.B., Bradfer-Lawrence, T., Lees, A.C., Vale, E.M., Barlow, J., 2024b. The efficacy of acoustic indices for monitoring abundance and diversity in soil soundscapes. Ecological Indicators 169, 112954. doi:10.1016/j.ecolind.2024.112954.

Oelze, M.L., O'Brien, Jr., W.D., Darmody, R.G., 2002. Measurement of attenuation and speed of sound in soils. Soil Science Society of America Journal 66, 788–796. doi:10.2136/sssaj2002.7880.

Pennekamp, F., Iles, A.C., Garland, J., Brennan, G., Brose, U., Gaedke, U., Jacob, U., Kratina, P., Matthews, B., Munch, S., Novak, M., Palamara, G.M., Rall, B.C., Rosenbaum, B., Tabi, A., Ward, C., Williams, R., Ye, H., Petchey, O.L., 2019. The intrinsic predictability of ecological time series and its potential to guide forecasting. Ecological Monographs 89, e01359. doi:10.1002/ecm.1359.

Phipson, B., Smyth, G.K., 2010. Permutation p-values should never be zero: calculating exact p-values when permutations are randomly drawn. Statistical Applications in Genetics and Molecular Biology 9, Article 39. doi:10.2202/1544-6115.1585.

Pieretti, N., Farina, A., Morri, D., 2011. A new methodology to infer the singing activity of an avian community: the acoustic complexity index (ACI). Ecological Indicators 11, 868–873. doi:10.1016/j.ecolind.2010.11.005.

Pijanowski, B.C., Villanueva-Rivera, L.J., Dumyahn, S.L., Farina, A., Krause, B.L., Napoletano, B.M., Gage, S.H., Pieretti, N., 2011. Soundscape ecology: the science of sound in the landscape. BioScience 61, 203–216. doi:10.1525/bio.2011.61.3.6.

Powsner, L., 1935. The effects of temperature on the durations of the developmental stages of *Drosophila melanogaster*. Physiological Zoology 8, 474–520. doi:10.1086/physzool.8.4.30151263.

Richard, T.L., Hamelers, H.V.M., Veeken, A., Silva, T., 2002. Moisture relationships in composting processes. Compost Science & Utilization 10, 286–302. doi:10.1080/1065657X.2002.10702093.

Roberts, D.R., Bahn, V., Ciuti, S., Boyce, M.S., Elith, J., Guillera-Arroita, G., Hauenstein, S., Lahoz-Monfort, J.J., Schröder, B., Thuiller, W., Warton, D.I., Wintle, B.A., Hartig, F., Dormann, C.F., 2017. Cross-validation strategies for data with temporal, spatial, hierarchical, or phylogenetic structure. Ecography 40, 913–929. doi:10.1111/ecog.02881.

Robinson, J.M., Breed, M.F., Abrahams, C., 2023. The sound of restored soil: using ecoacoustics to measure soil biodiversity in a temperate forest restoration context. Restoration Ecology 31, e13934. doi:10.1111/rec.13934.

Rubin, D.B., 1981. The Bayesian bootstrap. The Annals of Statistics 9, 130–134. doi:10.1214/aos/1176345338.

Savage, K.E., Davidson, E.A., 2003. A comparison of manual and automated systems for soil CO2 flux measurements: trade-offs between spatial and

temporal resolution. Journal of Experimental Botany 54, 891–899. doi:10.1093/jxb/erg121.

Schreiber, T., Schmitz, A., 1996. Improved surrogate data for nonlinearity tests. Physical Review Letters 77, 635–638. doi:10.1103/PhysRevLett.77.635.

Sethi, S.S., Bick, A., Ewers, R.M., Klinck, H., Ramesh, V., Tuanmu, M.N., Coomes, D.A., 2023. Limits to the accurate and generalizable use of soundscapes to monitor biodiversity. Nature Ecology & Evolution 7, 1373–1378. doi:10.1038/s41559-023-02148-z.

Shannon, C.E., 1948. A mathematical theory of communication. Bell System Technical Journal 27, 379–423, 623–656. doi:10.1002/j.1538-7305.1948.tb01338.x.

Siddagangaiah, S., Chen, C.F., Hu, W.C., Pieretti, N., 2019. A complexity-entropy based approach for the detection of fish choruses. Entropy 21, 977. doi:10.3390/e21100977.

Stroud, J.L., Kalkowski, M.K., Hassall, K.L., Treadway, M., Fannon, J., Keith, A., Ruiz, S., Attenborough, K., 2025. The use of ecoacoustics to monitor soil ecology: a critical review with reference to earthworms. European Journal of Soil Science 76, e70229. doi:10.1111/ejss.70229.

Sueur, J., Aubin, T., Simonis, C., 2008a. Seewave, a free modular tool for sound analysis and synthesis. Bioacoustics 18, 213–226. doi:10.1080/09524622.2008.9753600.

Sueur, J., Aubin, T., Simonis, C., 2025. seewave: sound analysis and synthesis, R package version 2.2.4. https://CRAN.R-project.org/package=seewave.

Sueur, J., Pavoine, S., Hamerlynck, O., Duvail, S., 2008b. Rapid acoustic survey for biodiversity appraisal. PLoS ONE 3, e4065. doi:10.1371/journal.pone.0004065.

Taylor, A.F., Breed, M.F., Abrahams, C., Annells, A., Bradfer-Lawrence, T., Cavagnaro, T., Görres, C.M., Gossner, M.M., Liddicoat, C., Linke, S., Metcalf, O.C., Roberts, L., Sørensen, L.V., Sun, X., Timperley, J.H., Robinson, J.M., 2026. Hums in the humus: opportunities and challenges for soil ecoacoustics. Trends in Ecology & Evolution 41, 355–367. doi:10.1016/j.tree.2025.12.007.

Theiler, J., Eubank, S., Longtin, A., Galdrikian, B., Farmer, J.D., 1992. Testing for nonlinearity in time series: the method of surrogate data. Physica D: Nonlinear Phenomena 58, 77–94. doi:10.1016/0167-2789(92)90102-S.

Villanueva-Rivera, L.J., Pijanowski, B.C., 2018. soundecology: soundscape ecology, R package version 1.3.3. https://CRAN.R-project.org/package=soundecology.

Villanueva-Rivera, L.J., Pijanowski, B.C., Doucette, J., Pekin, B., 2011. A primer of acoustic analysis for landscape ecologists. Landscape Ecology 26, 1233–1246. doi:10.1007/s10980-011-9636-9.

Virtanen, P., Gommers, R., Oliphant, T.E., Haberland, M., Reddy, T., Cournapeau, D., Burovski, E., Peterson, P., Weckesser, W., Bright, J., et al., 2020. SciPy 1.0: fundamental algorithms for scientific computing in Python. Nature Methods 17, 261–272. doi:10.1038/s41592-019-0686-2.

Ziv, J., Lempel, A., 1978. Compression of individual sequences via variable-rate coding. IEEE Transactions on Information Theory 24, 530–536. doi:10.1109/TIT.1978.1055934.

Supplementary Material

Hearing the heat: a proof-of-concept study of nonlinear sound measures for distinguishing phases of rapid organic decomposition

Jakob Eisenhauer

Part A: Supplementary Methods

S1 Purpose and structure

This Supplementary Material has three parts. Part A, the Supplementary Methods (Sections S1–S17), gives details of the methods described in the main text. Part B, the Supplementary Results (Sections S18–S24), gives further results of these analyses, including the figures and tables per configuration. Part C, the Supplementary Analyses (Sections S25–S27), reports analyses that the main text reports only in summary, each with its method and result. The five buckets were prepared from one material batch and replicate the measurement within one decomposition run, not the decomposition process (Hurlbert, 1984; main text, Section 3.6). The 40 acoustic windows of a recording increased temporal resolution, not the number of replicates, and the 80 measure-band trajectories are dependent analytical configurations, not 80 independent observations.

S2 Experimental material and containers

Buckets A–E were black, tapered polypropylene buckets with an upper diameter of 37 ± 0.5 cm, a lower diameter of 28 ± 0.5 cm and a height of 26.5 ± 0.5 cm. As a truncated cone, their volume was 22.1 ± 0.6 L, with the uncertainty from Gaussian error propagation. The buckets stood on about 10 cm of padding on the floor, at least 65 cm apart (centre to centre).

The vermicompost came from an active vermicomposting system and had been stored for nine months without feeding. Seven days before monitoring, it was reactivated by adding water to saturation and about 10 g of molasses per litre of vermicompost. Before mixing, the hay was soaked for about 12 h in water at 25–30 °C and then left to drain for 6 h, covered against evaporation.

S3 Measurement schedule and experimental events

Regular sessions (measurements 2–31) were scheduled at 13:00 (afternoon) and 21:00 (evening). The time of an occasion was its start time in the measurement protocol plus 30 min.

According to the recorder time stamps, the last of the five sequential recordings of an occasion started a median of 60 min after the first, always in the order A, B, C, D, E. Because the order never changed, a bucket's position in the sequence, and any drift of room noise within a session that is tied to it, is constant within the bucket and removed by the within-bucket standardisation (Section S9). What remains is the alternation of afternoon and evening sessions, with possible differences in room noise and building services, which was tested as an additional term of L (Section S27).

The repeatability of the probe thermometer was determined in a heat-bath test. The probe was placed in a water bath at 30 °C, and 25 readings were taken at 2 min intervals. Between readings the probe was switched off, brought to a higher temperature and returned to equilibrium in the bath, so that each reading followed a fresh equilibration. Readings ranged from 29.9 to 30.2 °C (mean 30.01 °C, SD 0.078 °C).

S4 Acoustic recording

The recorder was an ALLSOUNDER ALISO (model AS-ALISO, firmware 1.0.0) with the manufacturer-supplied piezoelectric soil sensor. Recordings were started manually and stored as single-channel 16-bit WAV files, with the input gain at 0 dB. The analysis compares temporal responses after within-bucket standardisation. It does not interpret absolute sound-pressure levels or transfer results to other sensor-coupling conditions. The discarded start of a recording (main text, Section 2.2) lasted a median of 2.8 min. Each analysed excerpt was required to contain exactly 600 s at 48 kHz without non-finite values.

S5 Frequency decomposition and temporal scales

The band-pass filters (main text, Section 2.2) were represented as second-order sections and applied forward and backward, and the filtered series was resampled by a rational polyphase filter. The local RMS series $r(t)$ was computed on the full 600 s band-passed signal, before the division into 15 s windows, as the square root of the mean of x^2 over a centred window, with reflection at the boundaries. Its width of $5\lambda f_s/f_{\min}$ samples (main text, Section 2.2), increased by one sample where necessary to make it odd, equals ten times the delay τ in every band and spans 15 cycles of $f_{\min}$ in the lowest and 1.3 in the highest band. The same τ was used as the ordinal-pattern delay for PE and as the decimation interval for LZC78, RSE_4, and RSR. Because λ decreases by a factor of $\sqrt{2}$ per octave, the physical delay τ/f_s scales approximately as $f_{\max}^{-3/2}$.

S6 Quantiser construction

Scalar quantisers were fitted separately for every bucket, octave band, and RMS-window width, but were shared across all measurement occasions and both session times within that combination. Each recording contributed 4 000 evenly spaced RMS values, or all available values when fewer were present. Pooling equal numbers of support values per recording prevented recordings with more RMS values from dominating the boundaries. For alphabet size A, the 1st and 99th percentiles of the pooled support values defined the robust central range. $A - 1$ equally spaced internal boundaries divided that range, and

values below or above it entered the two outermost bins. A control with quantisers fitted per recording is described in Section S27.9.

S7 Nonlinear acoustic measures

S7.1 Permutation entropy

For each RMS window, order-4 delay vectors $[r_t, r_{t+\tau}, r_{t+2\tau}, r_{t+3\tau}]$ were replaced by their ordinal permutation (Bandt and Pompe, 2002). Tied values were ordered by their original position (stable sorting). Bandt and Pompe (2002) instead suggest perturbing tied data. If p_j is the observed frequency of the jth of 4! possible patterns, the reported value was

$$\mathrm{PE} = -\frac{1}{\ln(4!)} \sum_j p_j \ln p_j, \tag{S1}$$

using only positive empirical probabilities, with no pseudocount added.

S7.2 LZ78 phrase count

The $A = 100$ symbol sequence was decimated by τ and parsed from left to right with an incremental LZ78 prefix-symbol dictionary (Ziv and Lempel, 1978). A new phrase was counted whenever the current prefix followed by the next symbol was absent from the dictionary. A non-empty terminal prefix was counted as the final, potentially incomplete phrase. LZC78 is the resulting phrase count c, not normalised by sequence length. Unlike the plug-in entropies of RSE_4, which are biased unless the sequence is much longer than the number of possible words and thus use a coarse alphabet ($A = 10$), the phrase count does not approach a limit. It keeps rising with sequence length, less steeply for more regular sequences, and is only compared between windows of equal length. Convergence is therefore not required, and a finer amplitude resolution ($A = 100$) was used.

S7.3 Relative sequence entropy and redundancy (RSE_k, RSR)

From the decimated $A = 10$ sequence, H_1 was the base-2 empirical entropy of individual symbols and H_k the empirical entropy of overlapping k-symbol words, with $k = 4$ in the primary analysis. Unobserved words had zero probability and did not contribute. RSR used the same decimated $A = 100$ sequence and LZ78 phrase count c as LZC78, with the finite-sequence entropy-rate proxy $h_{\mathrm{LZ}} = c \log_2(c)/N$ (Ziv and Lempel, 1978) and H_1 calculated from the same symbols. Both statistics (main text, Eq. 1) are undefined when $H_1 = 0$. Dividing by H_1 rather than by the maximum entropy relates the entropy rate to the symbol variety actually present in a window. With the block estimate of the entropy rate, $h_k = H_k/k$,

$$\mathrm{RSE}_k = \frac{kH_1 - H_k}{(k-1)H_1} = \frac{k}{k-1}\left(1 - \frac{h_k}{H_1}\right), \qquad \mathrm{RSR} = 1 - \frac{h_{\mathrm{LZ}}}{H_1}, \tag{S2}$$

so RSE_k is the block-estimate counterpart of RSR, rescaled by $k/(k-1)$. Neither estimator is exactly calibrated in finite samples. Finite-sample entropy bias and changes in the marginal symbol probabilities affect both, and the asymptotic argument behind h_{LZ} motivates but does not directly validate this finite-window proxy. Unlike the phrase count

itself, h_{LZ} is read as an entropy rate and converges slowly, the more slowly the larger the alphabet. RSR therefore depends more than LZC78 on the shared alphabet of 100, and alphabets of 50 and 200 were tested for both in the sensitivity analysis (Table S1).

S8 Conventional acoustic measures

The conventional measures were calculated from each filtered 15 s band signal. Except for AEI, spectral quantities used a short-time Fourier transform with 512-sample Hann frames, a 512-sample hop, no padding, and no boundary extension. Only bins between the lower and upper band edges were retained, and magnitudes were averaged across time frames to obtain the mean amplitude spectrum.

Log band energy was $10 \log_{10}(\max(\langle x^2 \rangle, 10^{-20}))$. ACI was the sum across frequency bins of the absolute first differences in magnitude across frames divided by the total magnitude in that bin, with bins at or below 10^{-20} contributing zero (Pieretti et al., 2011). Temporal and spectral entropy were the normalised Shannon entropies of the absolute Hilbert envelope and of the mean amplitude spectrum, respectively (Sueur et al., 2008b). Spectral flatness was the geometric mean divided by the arithmetic mean of the mean amplitude spectrum, after scaling by its maximum and flooring relative amplitudes at 10^{-6}, following the `sfm` function of the R package seewave (Sueur et al., 2008a, 2025).

The band-limited AEI variant used a separate no-overlap Hann spectrogram with a nominal 10 Hz frequency resolution. Each octave was divided into ten equally wide linear-frequency bins. For each bin, the proportion of time-frequency magnitudes above −50 dB relative to the maximum magnitude of that 15 s band window was calculated. AEI was the uncorrected Gini coefficient of the ten proportions (Villanueva-Rivera et al., 2011; Villanueva-Rivera and Pijanowski, 2018). Both edges were included in adjacent frequency masks, so bins on shared boundaries can contribute to both neighbours. This preserves the logic of the original AEI but is not the original broadband 1 kHz-bin definition.

ACI, AEI and the two entropies were designed for broadband spectra and partly lose their meaning within one octave, whereas the RMS window and delay of the nonlinear measures were scaled to each band. As a reference, the six conventional indices were also computed for one broadband signal, band-pass filtered from 64 to 16384 Hz (same filter, no resampling at 48 kHz), with the same 15 s windows, median aggregation and standardisation. Standard parameters were used. ACI followed soundecology (Pieretti et al., 2011; Villanueva-Rivera and Pijanowski, 2018): 512-sample Hamming frames without overlap and temporal clusters of 5 s (three per window), summed over all frequency bins between 64 and 16384 Hz and over the clusters. AEI used the soundecology defaults (Villanueva-Rivera et al., 2011; Villanueva-Rivera and Pijanowski, 2018): a spectrogram with 10 Hz resolution, −50 dB relative to the maximum, and ten 1 kHz bins up to 10 kHz. Spectral entropy and spectral flatness were computed from the mean spectrum of 512-sample Hann frames between 64 and 16384 Hz, temporal entropy from the Hilbert envelope, and log band energy as above. Models, cross-validation and the same temperature surrogates were applied to these six configurations.

S9 Response and covariates

The within-bucket standardisation (main text, Section 2.3) used the mean and standard deviation over all available occasions of a bucket, including the baseline. It is a fixed transformation, not a fitted random-intercept model, and uses no information from other buckets. Centring without scaling was tested in the sensitivity analysis (Section S14). For the fit to the mean trajectory, the response at an occasion was the unweighted mean of the standardised values over the available buckets, and the temperature the mean of the bucket temperatures. The cross-validation used the bucket values directly.

Elapsed time was calculated in days from the start of monitoring and centred. Internal temperature entered as $T_{si} - 30\,°\mathrm{C}$, the bucket's own reading in the cross-validation and the five-bucket mean in the fit to the mean trajectory. The cooling indicator C_i was 1 for occasions after the maximum of the mean temperature, taken over the five buckets in the fit to the mean trajectory and over the four training buckets in every cross-validation fold, also for the held-out bucket. With the real temperature, both maxima fell at measurement 5 (cooling occasions: measurements 6–31).

S10 Models and fitting

S10.1 Ordinary least-squares models

Time-only, temperature-only, L and $\mathrm{L}_{\mathrm{time}}$ (main text, Eqs. 2–5) were fitted by ordinary least squares, separately for every configuration, with coefficients not sign constrained. In the fit to the mean trajectory ($n = 31$), they were summarised by $R^2 = 1 - \mathrm{RSS}/\mathrm{TSS}$. Information criteria such as AICc were not used for model comparison, because they assume independent errors and the residuals were autocorrelated (Section S25).

S10.2 Data-driven shared curve (NP)

NP (main text, Eq. 6) is a Nadaraya–Watson kernel smoother (Nadaraya, 1964; Watson, 1964), a moving average of a mean trajectory over time with Gaussian weights. Missing occasions were masked, so that the kernel weights were renormalised over the available ones. In every cross-validation fold, the curve was computed from the raw mean of the four training buckets and used directly as the prediction of the held-out bucket, without a fitted amplitude factor. The bandwidth was chosen from $s \in \{0.4, 0.75, 1.0, 1.5, 2.0, 3.0, 4.0\}\,\mathrm{d}$ by an inner leave-one-bucket-out cross-validation within the four training buckets (each predicted by the smoothed mean of the other three), as the value with the smallest squared error summed over all 80 configurations, so one s applies to all configurations of a fold. Selecting s per configuration gave noisy choices and no gain. For the fit to the mean trajectory, $s = 0.75\,\mathrm{d}$, chosen in the same way on all five buckets, was applied to the five-bucket mean. The trace of the smoother matrix gives 8.8 effective degrees of freedom, against 4 parameters of L. The unsmoothed mean of the training buckets (Section S18) is the limiting case $s \to 0$.

S10.3 Bayesian bootstrap

All uncertainty intervals of fits and coefficients used the two-level extension of the Bayesian bootstrap described in the main text (Section 2.5; Rubin, 1981): the bands of the fits to the

mean trajectory (main text, Figs. 1 and 6) and the coefficient distributions and intervals by band (main text, Fig. 4; all measures: Section S21). The weights were Dirichlet(1), and equal weights give the plain median and mean of the main analysis. Temperature and the cooling indicator were those of the observed five-bucket mean, and NP was refitted with s fixed. The coefficient estimates are those of the fit to the observed mean trajectory. Counts of coefficient intervals that exclude zero (main text, Section 3.3) summarise them across bands and measures descriptively, without correction for multiple comparisons (main text, Section 3.6).

S11 Cross-validation

In every fold, the training data stacked all occasions of the four remaining buckets (up to 124 rows), each with its own temperature. Leave-one-bucket-out cross-validation matches the structure of the data, in which occasions within a bucket are autocorrelated, while buckets are separate physical units (Roberts et al., 2017).

S12 Temperature-surrogate procedure

The IAAFT surrogates of the mean temperature course (31 occasions; Schreiber and Schmitz, 1996) started from a random permutation of the course. The Fourier amplitudes of the real course were imposed while the current phases were kept, and the result was rank-matched to the sorted real values, until the series no longer changed (at most 1 000 iterations). For every surrogate, the cooling indicator was re-derived from the peak of the surrogate (Section S9). The full cross-validation of temperature-only, L_{time} and L was repeated on all 80 configurations. The same 100 000 surrogates were used for all configurations, models and groups, so that the correlation between configurations is preserved in the null distribution.

The conditional test used the 3 298 surrogates whose cooling indicator was identical to the real one in all five folds, with p computed as in the main text over these 3 298 surrogates.

S13 Bucket agreement and redundancy

For bucket agreement (main text, Section 2.5), the Spearman correlation of two buckets was computed over the occasions recorded in both. The median over the ten pairs was summarised by the median over the configurations of a group. Redundancy was computed over the within-bucket standardised bucket-occasion values of all 80 configurations, within and between bands (main text, Fig. 5).

For the cross-prediction between the groups, every configuration of one group (target) was predicted from all configurations of the other group (predictors: 48 conventional or 32 nonlinear) by ridge regression on the same values, with leave-one-bucket-out cross-validation (Section S11) and the held-out skill of the main text. Predictors were standardised and targets centred with the statistics of the training buckets. The penalty was chosen for every target from 31 values (10^{-2} to 10^{4} times the number of training rows, logarithmically spaced) by a second leave-one-bucket-out within the four training buckets, so the held-out bucket did not enter its choice. In a variant, the predictors from

the target's own octave band were removed (42 conventional or 28 nonlinear predictors), which separates redundancy within a band from information shared across bands.

S14 Sensitivity scenarios

Sensitivity runs recomputed the window values for alternative preprocessing settings (Table S1) and reused the main values for unaffected measures. Low and high alternatives changed one parameter at a time. For RSE_4, alphabets of 8 and 12 roughly halve and double the number of possible 4-symbol words ($8^4 = 4\,096$ and $12^4 = 20\,736$ against 10^4). Block lengths of 3 and 5 change it tenfold. Combined stress scenarios changed window length, lambda multiplier, RMS width, LZC alphabet, PE order, RSE block length, and RSE alphabet simultaneously (the lambda exponent was tested separately). One further scenario kept the main window values but only centred them within each bucket, without dividing by the bucket's standard deviation, so that buckets with a larger spread weighed more in the training fits. Skill was still computed around the held-out bucket's own mean. For every scenario, the complete cross-validation of all models was repeated (results: Section S20). The surrogate test was not repeated.

Table S1: Parameter sensitivity grid. Low and high alternatives changed one parameter at a time from the primary setting. The standardisation has one alternative only.

Parameter	Primary	Low	High	Affected measures
Window length and step	15 s	7.5 s	30 s	All ten
Lambda multiplier	1	0.5	2	All four nonlinear
Lambda exponent	−0.5	−0.25	−1.0	All four nonlinear
RMS width factor κ ($\kappa\lambda/f_{\min}$)	5	2.5	10	All four nonlinear
LZC alphabet	100	50	200	LZC78 and RSR
PE order	4	3	5	PE
RSE block length	4	3	5	RSE_4
RSE alphabet	10	8	12	RSE_4
Within-bucket standardisation	mean and SD	mean only		All ten

S15 Mass and moisture balance: methods

S15.1 Measurements

Each bucket was weighed with its contents before and after the experiment on a KERN HCB 50K20 balance (0.02 kg display increment), and the empty buckets and all moisture samples on a KERN EMB 5.2K1 (1 g). Water fractions were determined by drying at 60 °C for 48 h. The vermicompost was sampled once before mixing, with 615 g fresh and 243 g dry mass, giving a water fraction of 0.605. The hay was weighed before (3.82 kg) and after soaking (12.98 kg). Its moisture before soaking was not measured. It was represented by $q \sim \text{Triangular}(0.05, 0.075, 0.11)$, informed by DWD station 03284 observations (Deutscher Wetterdienst, 2026) and published hay equilibrium-moisture relationships (Brown, 2015; Johnson, 2022). Assuming no dry-matter loss during soaking, the hay dry mass was $m_{\text{pre}}(1-q)$ and the water fraction of the soaked hay $1 - m_{\text{pre}}(1-q)/m_{\text{post}}$ (0.73 at the mode of q). With the mixing ratio, the initial water fraction of the substrate

was 0.65. At the end, one sample of 476–610 g fresh mass was taken from each bucket. In bucket B, a sample from the top and one from the bottom layer were taken and combined. The resulting water fractions and masses are listed in Table S4. The standard uncertainty of how well one sample represents a bucket was set to half the top-bottom difference in bucket B, 0.007, for all buckets.

S15.2 Balance model

Every reading carried the manufacturer's repeatability (normal) and linearity and display-rounding terms (uniform): for the HCB, SD 20 g, ±40 g and ±10 g; for the EMB, SD 1 g, ±3 g and ±0.5 g (KERN & Sohn GmbH, 2026). Each sampled tare was reused for the paired before and after masses of its bucket. The mixing ratio (2.00 ± 0.02) entered as a further input. For each bucket, with initial mass M_0 and water fraction w_0, final mass M_1 and water fraction w_1,

$$D_0 = M_0(1 - w_0), \quad D_1 = M_1(1 - w_1), \quad L_d = D_0 - D_1, \quad \Delta W = M_1 w_1 - M_0 w_0. \quad \text{(S3)}$$

The direct estimate of dry-mass loss was L_d. The retained-water estimate $L_w = \Delta W / Y$ converted the water gained into oxidised dry matter with one metabolic-water yield $Y \sim \text{Triangular}(0.48, 0.556, 0.62)\,\text{kg kg}^{-1}$ per Monte Carlo draw, in line with the 0.5–0.6 g of metabolic water per g of volatile solids decomposed reported for composting (Richard et al., 2002). The mode follows complete cellulose oxidation. Theoretical yields are 0.41, 0.60 and 1.07 kg kg^{-1} for protein, carbohydrate and fat (EFSA Panel on Dietetic Products, Nutrition, and Allergies, 2010), so the interval spans carbohydrate-dominated oxidation with a considerable protein contribution. It was set to exclude a fat-dominated substrate because no fat was added. Evaporation was minimised by the cover and not measured. Any residual evaporation, through gas exchange and the brief openings, would bias L_w downward (Richard et al., 2002). The two estimates share inputs, are not independent lines of evidence and were not combined. Losses are given as the ratio of pooled loss to pooled initial dry mass of the five buckets, from 200 000 Monte Carlo draws. The balance cannot allocate the loss among hay, vermicompost, microbes, fauna, leaching or respiration.

S16 Faunal observations

Organisms observed opportunistically were provisionally assigned to *Drosophila* sp. (Drosophilidae), *Lucilia* sp. (Calliphoridae), *Eisenia* or *Dendrobaena* sp. (Lumbricidae) and *Coboldia* sp. (Scatopsidae). During the experiment, adult *Drosophila* and blowflies (*Lucilia* sp.) appeared in the laboratory. The notes in the measurement protocol place this between measurements 15 and 26 (days 7.1–12.8 of the time axis of the models). When the buckets were emptied at the end of the experiment, earthworms were found in every bucket, together with earthworm cocoons, and *Coboldia* sp. in large numbers underneath the buckets. Because searches and counts were not standardised, these observations document presence only. They were not used to infer abundance, bucket differences, or acoustic source identity.

S17 Reproducibility and exported data

The analysis was implemented in Python with NumPy, pandas, SciPy and SoundFile, Numba for optional acceleration and Matplotlib for figures. The code is organised in modules for the acoustic measures (`audio_measures.py`), the signal-level surrogates (`signal_surrogates.py`), the models and cross-validation (`models.py`), the model comparison, temperature-surrogate test, diagnostics and further checks (`analysis.py`), the Bayesian bootstrap (`bootstrap.py`), the level-invariant control (`loudness_control.py`), the mass balance (`mass_balance.py`), tables and figures. The code (Eisenhauer, 2026a) and the data (Eisenhauer, 2026b) are archived on Zenodo. `run_all.py` runs all steps, and the repository README lists the figures and tables each step produces. All settings are collected in `settings.py`, and random seeds are fixed.

Part B: Supplementary Results

S18 Fit and held-out skill per configuration

Using the mean of the four training buckets directly as the prediction of the held-out bucket, the limiting case $s \to 0$ of NP, gave a median skill of 0.41 for the nonlinear and 0.03 for the conventional configurations. Figs. S1–S4 show the fits and the held-out skill per configuration, by band and by measure.

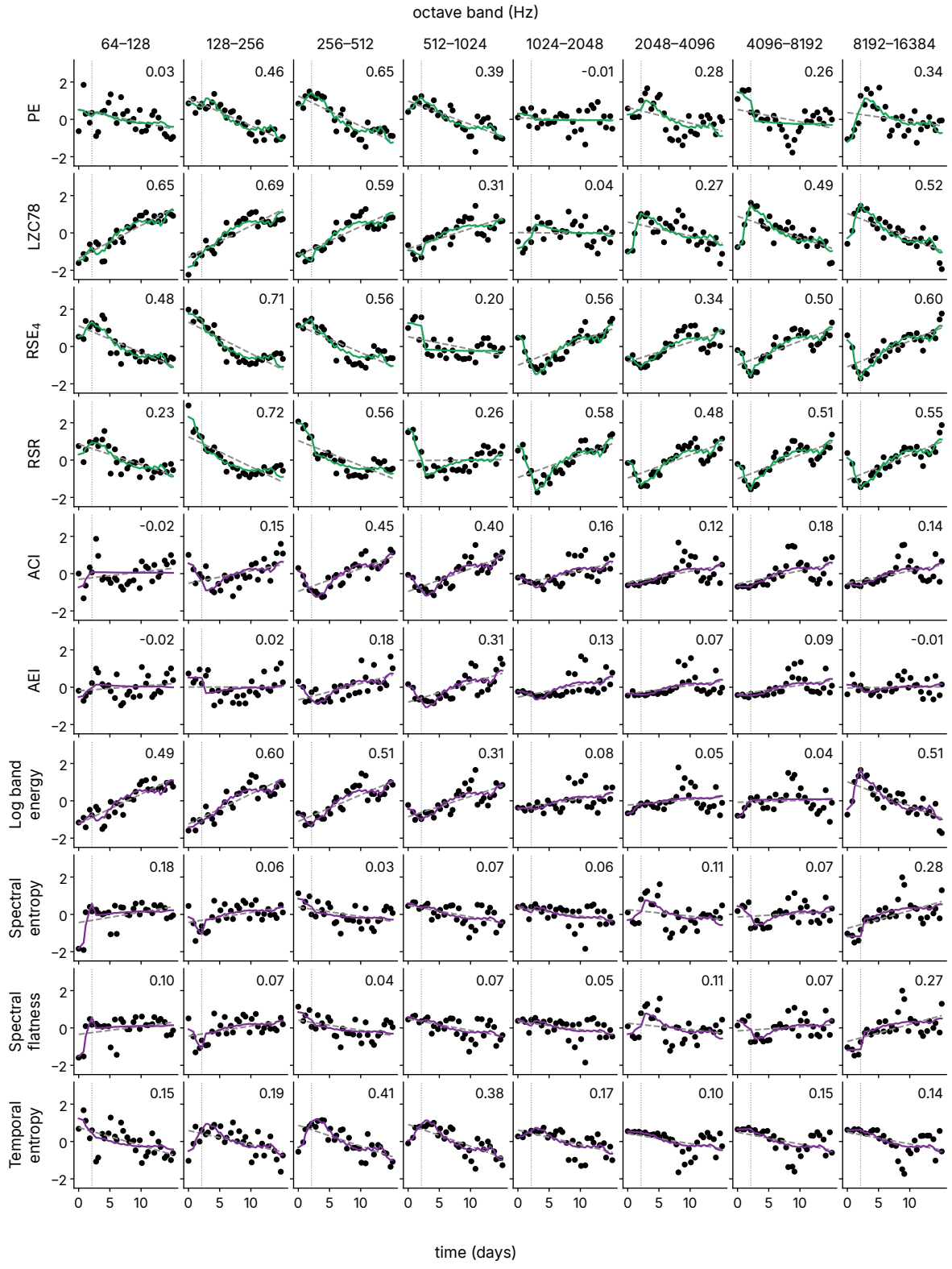


Figure S1: All 80 configurations: rows are measures (nonlinear above, conventional below), columns octave bands. Black points: mean of buckets A–E; green (nonlinear) and purple (conventional) line: fit of model L to the mean trajectory; dashed line: time-only fit; dotted line: temperature peak. The number in each panel is the held-out skill of L.



Figure S2: Held-out skill of model L for every measure and band (a), and its difference from the time-only model (b) and from L_{time} (c). Measures above the black line are nonlinear. Values are single configurations evaluated on the same five buckets and should be read as patterns across neighbouring bands and related measures. The descriptive surrogate p-value of every configuration is listed in the exported table `02_cv_per_config.csv`.

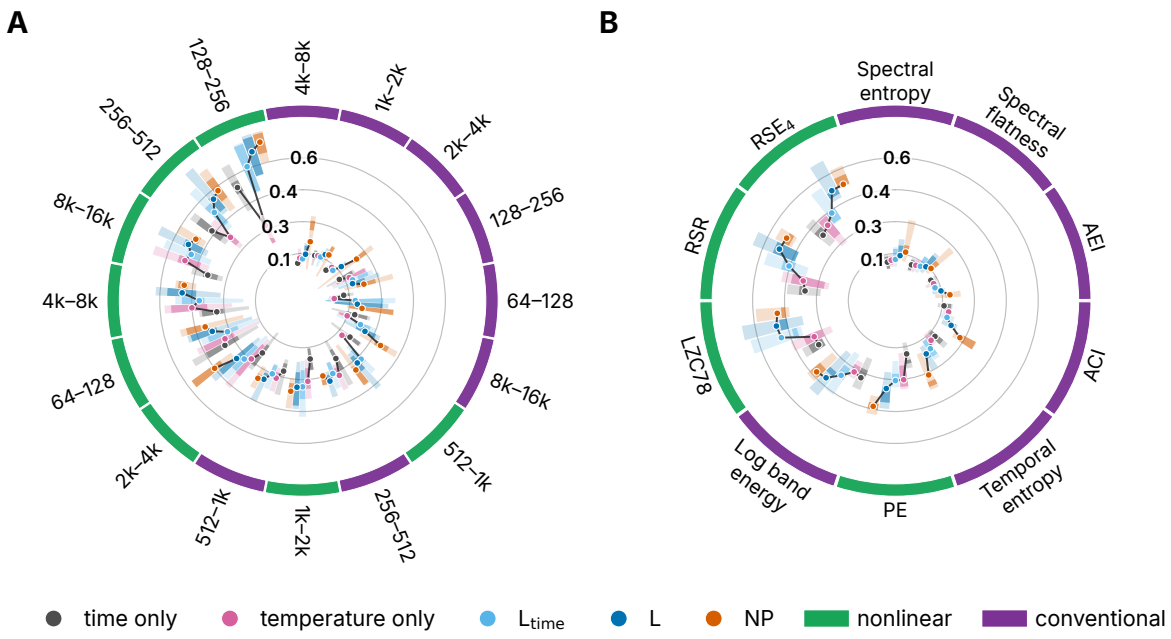


Figure S3: Median held-out skill of the five models, (A) by octave band and (B) by measure, separately for the nonlinear (green ring) and conventional configurations (purple ring). Categories are sorted clockwise from the top in ascending order of the skill of L. NP: main text, Section 3.5. Points: median over the configurations of a category of the skill averaged over the five folds; light bars: range over the five held-out buckets; dark bars: second to fourth of the five.

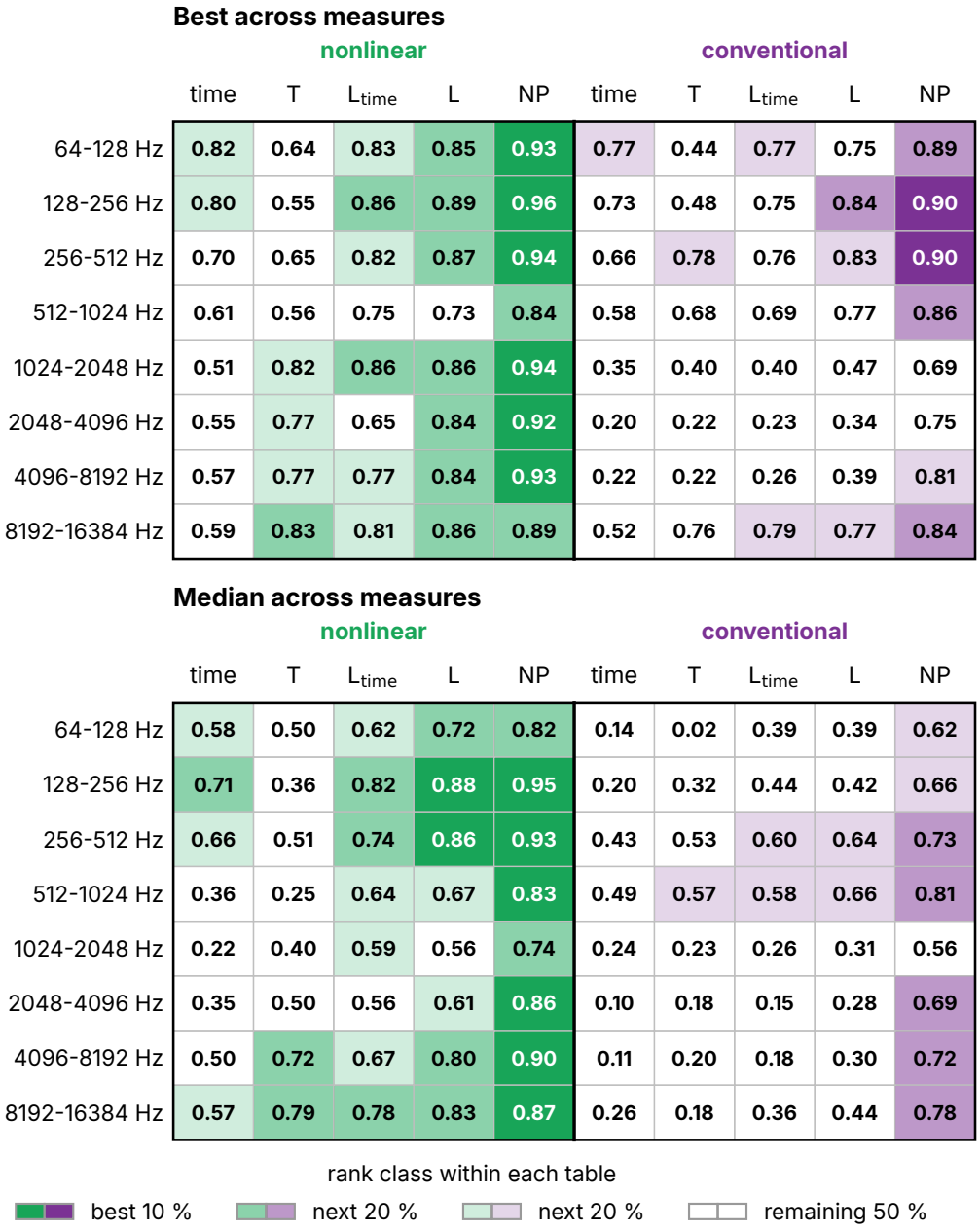


Figure S4: Fit to the mean trajectory (R^2) per octave band for the five models (time: time-only; T: temperature-only), best (top) and median configuration (bottom) of each group; companion of main-text Fig. 3, which shows held-out skill for L and NP only. NP has about 8.8 effective degrees of freedom against 2–4 parameters of the other models, so its in-sample R^2 is not comparable with theirs. Shading ranks the cells within each table.

S19 Temperature-surrogate results

For the group difference of L (primary test; main text, Section 3.2), the 95th percentile of the surrogate differences was 0.283. Descriptive results not given in the main text are the group difference for temperature-only ($p = 0.021$) and L_{time} in the conventional group ($p = 0.68$). Single configurations are shown in Fig. S2.

For the conventional group, the conditional surrogate median was 0.07 (95th percentile 0.13) against the observed 0.12 ($p = 0.078$). The nonlinear group is reported in the main text, Section 3.2. These surrogates resembled the real course more closely than the unrestricted ones (main text, Section 3.2) and set a harder benchmark, so the conditional p-values are conservative.

IAAFT assumes that the end of a series joins its start. The real course ended 1.7 °C below its start (range about 13 °C), so this assumption caused only a small jump. The surrogates were not near-copies of the real course. Their correlation with it had a median of −0.10 (interquartile range −0.39 to 0.40), only 1.1% had a correlation of 0.9 or more, and 3% peaked at measurement 5. The null distribution of L is bimodal (main text, Fig. 2). Many surrogates whose peak falls early in the series reach a skill close to that of the time-only model, because a cooling offset and a temperature slope can then reproduce part of a smooth trend.

S20 Sensitivity results

Centring without scaling lowered the median skill of L slightly for the nonlinear measures (0.467 against 0.485) and more for the conventional indices (0.063 against 0.124), most for AEI and spectral entropy (Fig. S6).

Table S2: Median held-out skill for every preprocessing scenario (Section S14), by measure group, for time-only, L_{time} and L. Conventional cells are left blank where a parameter does not affect the conventional measures (all but window length and centring). Their values are then those of the primary analysis.

	Nonlinear			Conventional		
Scenario	time-only	L_{time}	L	time-only	L_{time}	L
primary analysis	0.329	0.397	0.485	0.067	0.084	0.124
window 7.5 s	0.330	0.400	0.480	0.078	0.101	0.136
window 30 s	0.326	0.428	0.498	0.061	0.075	0.113
lambda multiplier 0.5	0.352	0.439	0.478			
lambda multiplier 2	0.279	0.318	0.410			
lambda exponent -0.25	0.259	0.356	0.423			
lambda exponent -1.0	0.310	0.448	0.481			
RMS width $2.5\lambda/f_{\min}$	0.275	0.362	0.404			
RMS width $10\lambda/f_{\min}$	0.344	0.435	0.484			
LZC alphabet 50	0.329	0.437	0.475			
LZC alphabet 200	0.298	0.376	0.436			
PE order 3	0.325	0.397	0.485			
PE order 5	0.332	0.397	0.485			
RSE block length 3	0.333	0.422	0.495			
RSE block length 5	0.328	0.392	0.485			
RSE alphabet 8	0.321	0.422	0.486			
RSE alphabet 12	0.333	0.412	0.485			
combined low	0.324	0.425	0.466			
combined high	0.284	0.356	0.440			
centring only (no SD scaling)	0.305	0.393	0.467	0.028	0.040	0.063

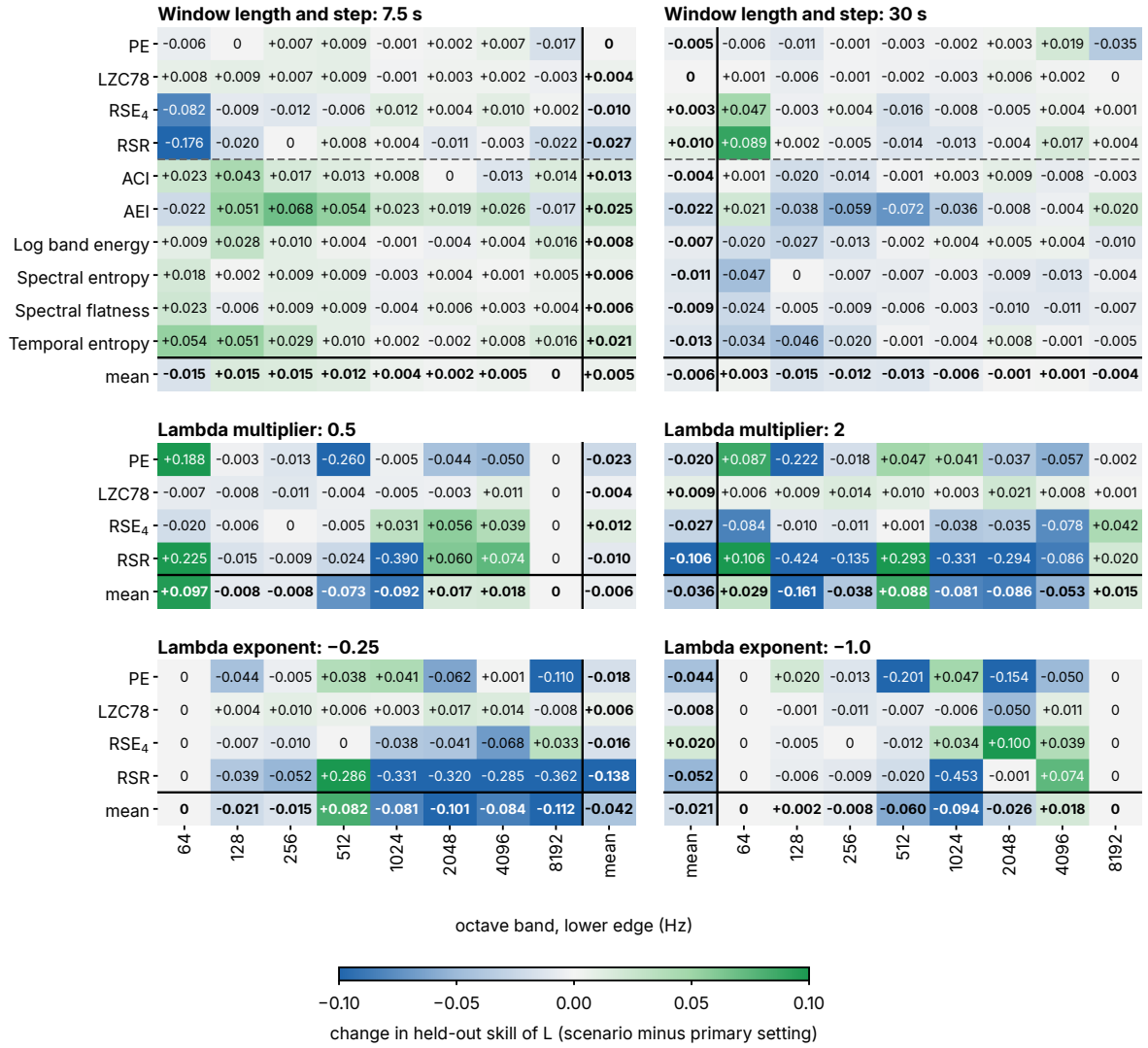


Figure S5: Change in held-out skill of L for every configuration in each low (left) and high (right) alternative of the sensitivity grid (Table S1), scenario minus primary setting: window length, lambda multiplier and lambda exponent (continued on the next page). Only measures affected by a parameter are shown. Row and column means are over the cells shown. Colours are clipped at ±0.1.

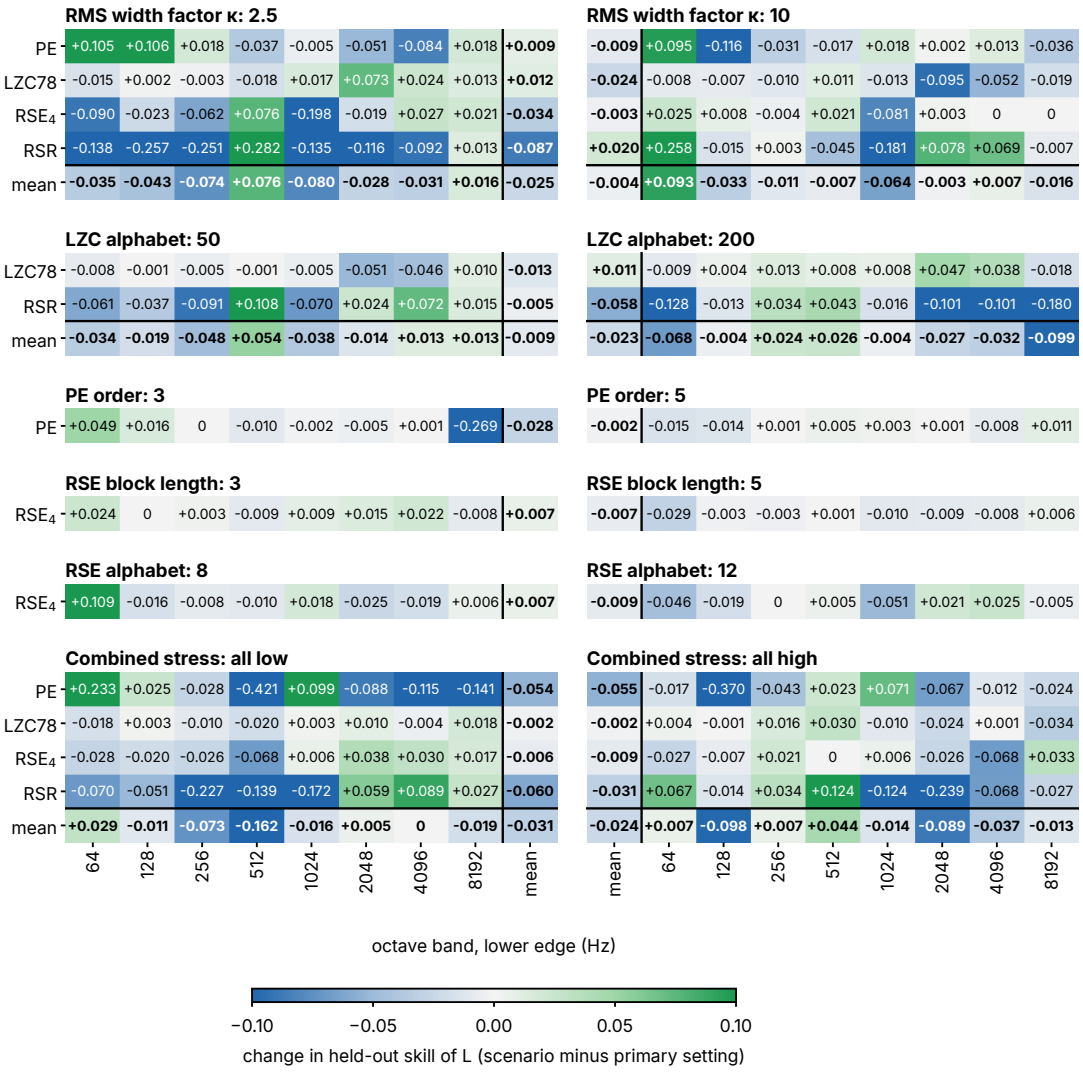


Figure S5: (continued) RMS width factor, LZC alphabet, PE order, RSE block length, RSE alphabet and combined stress.

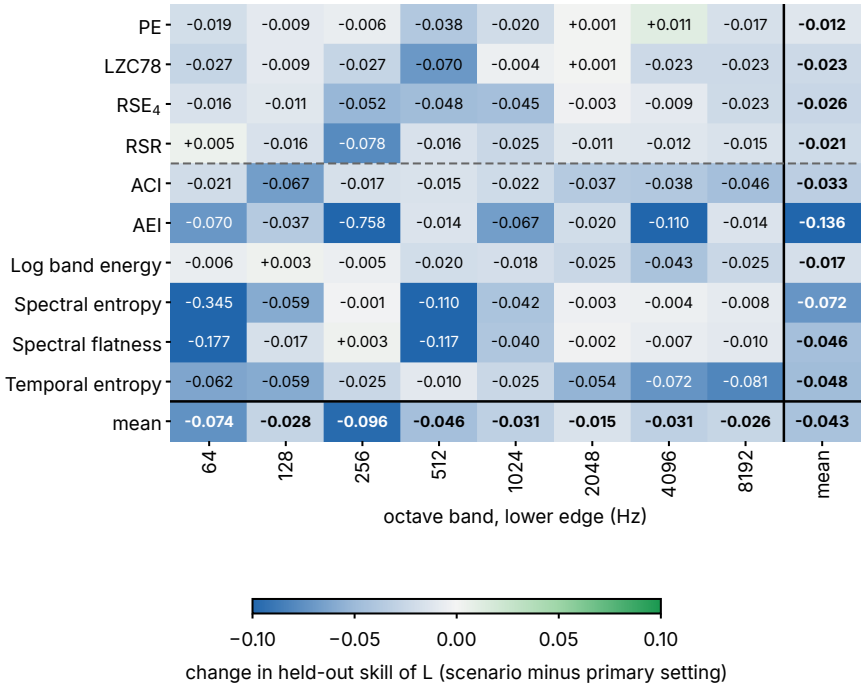


Figure S6: Change in held-out skill of L for every configuration when the window values were only centred within each bucket, without dividing by the bucket's standard deviation (Table S1), scenario minus primary setting. Means as in Fig. S5. Colours are clipped at ±0.1 (largest change −0.76, AEI at 256–512 Hz).

S21 Coefficients of L

Beyond the patterns described in the main text (Section 3.4), the slope change e of RSR was positive below and negative above about 1 kHz and PE had a negative cooling offset b in seven of eight bands (Fig. S7). The 95% Bayesian-bootstrap interval of d excluded zero in 19 of 32 nonlinear and 25 of 48 conventional configurations (b and e: main text, Section 3.3). Estimates and intervals of all cells are in the exported table `L_coefficients_bayes_boot.csv`.

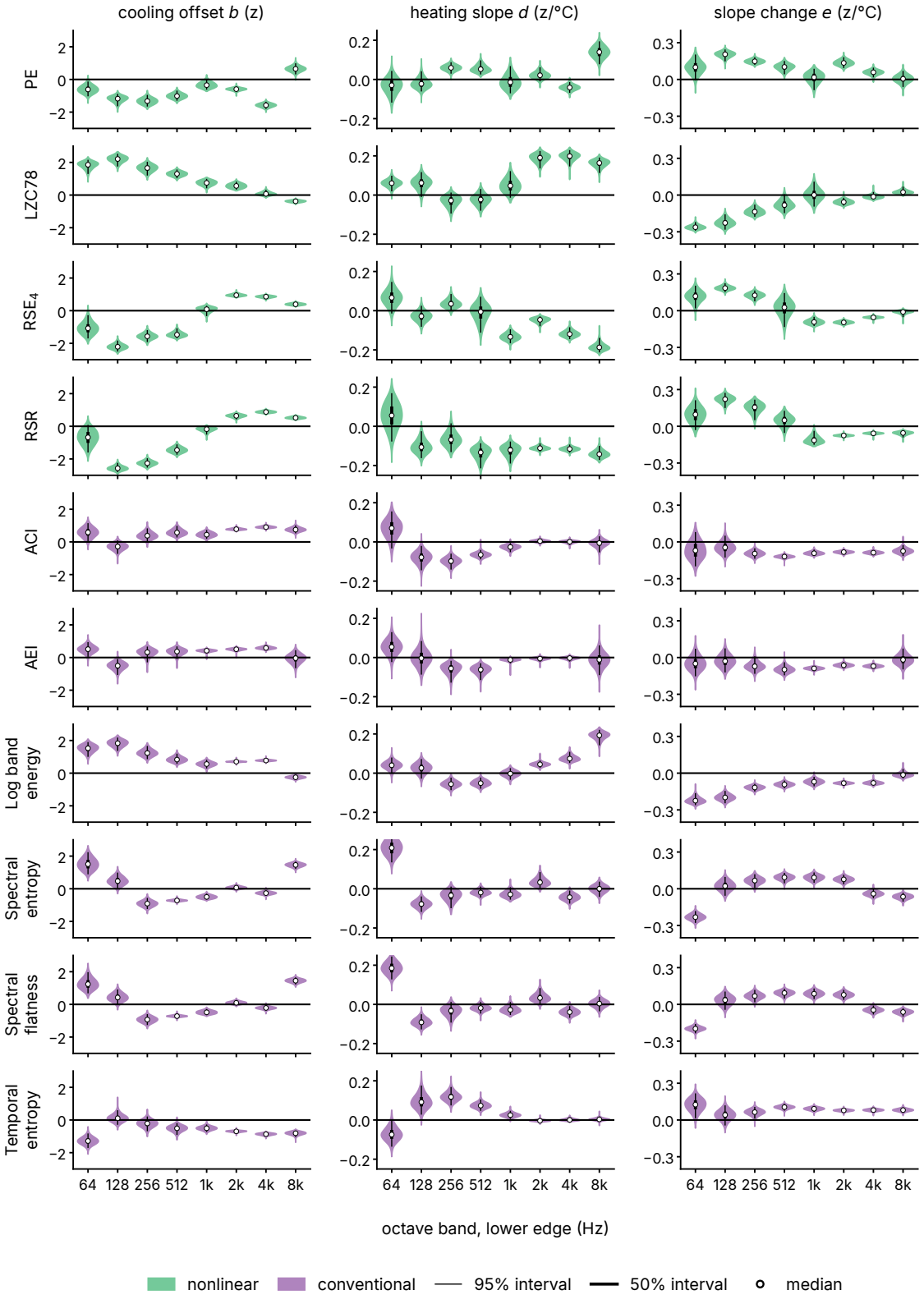


Figure S7: Coefficients of L by octave band for all ten measures (rows; nonlinear above): cooling offset b, heating slope d and slope change after the peak e (columns). Violins: distribution over the Bayesian bootstrap draws (Section S10.3); thin and thick bars: 95 and 50% intervals; white dot: median. The y axis is shared within each coefficient and set by the nonlinear measures, so violins that extend beyond it are cut at the panel edge.

S22 Redundancy

Besides the pairs named in the main text (Section 3.4), $|\rho| \geq 0.95$ was reached by ACI and temporal entropy (negatively correlated) in five bands, PE and log band energy in one band, RSE_4 and RSR in three bands (128–256, 4096–8192 and 8192–16384 Hz), and LZC78 with RSE_4 at 256–512 and 8192–16384 Hz and with RSR at 8192–16384 Hz (negative correlations). With log band energy of the same band, 5 of the 32 nonlinear measure-band pairs reached $|\rho| \geq 0.95$ and 12 reached $|\rho| \geq 0.85$.

Spectral entropy and spectral flatness are nearly redundant for nearly flat spectra. Writing the mean amplitude spectrum of a band as $a_j = \bar{a}(1 + \varepsilon_j)$ over N frequency bins, with relative variance $v = N^{-1} \sum_j \varepsilon_j^2$, a second-order expansion gives the normalised spectral entropy $H \approx 1 - v/(2 \ln N)$ and the spectral flatness $F \approx \exp(-v/2) \approx 1 - v/2$. Both decrease with the same quantity v, so their ranks nearly coincide. For strongly structured spectra the higher-order terms differ. A single near-silent bin drives F towards zero but changes H only slightly. The observed spectra were close to the flat regime, with median H of 0.987 to 0.997 and median F of 0.955 to 0.988 across bands. N was 26 frequency bins in the six lowest bands and 44 and 87 in the two highest. The values of v implied by H and by F agreed to within about 12%. Both measures are also independent of the spectrum's level, consistent with the finding that, unlike the level-dependent measures, they were not correlated between adjacent bands.

In the cross-prediction between the groups (Section S13), the median held-out skill was 0.85 (range 0.35–0.97) for the nonlinear measures predicted from the conventional indices and 0.65 (0.04–0.97) in the reverse direction. Without the predictors of the target's own band, it was 0.72 (0.10–0.91) and 0.55 (−0.01–0.90), so most of the shared information was not confined to a band. Among the targets, PE was the least predictable nonlinear measure (median 0.73; 0.38 without its own band, against 0.72–0.81 for LZC78, RSE_4 and RSR). Spectral entropy, spectral flatness and AEI were the least predictable conventional indices, with 0.32, 0.35 and 0.40 without their own band.

S23 Broadband conventional indices

Computed broadband with standard parameters (Section S8), the conventional indices predicted held-out buckets better than their octave-band versions (Table S3), with median skills of 0.15 for time-only, 0.12 for temperature-only and 0.18 for L_{time}. The median skill of L, however, was not distinguishable from the surrogates (surrogate median 0.15, 95th percentile 0.24, $p = 0.11$, descriptive). ACI, AEI and the spectral measures gained most from the broadband calculation, whereas broadband log band energy predicted poorly. The median skill of the nonlinear measures (0.48) exceeded the broadband conventional median by 0.26. With the surrogates, this difference had a median of 0.13 (95th percentile 0.21, $p = 0.003$, descriptive).

Table S3: Conventional indices computed broadband (64–16384 Hz, standard parameters; Section S8) compared with their octave-band versions. R^2: fit of L to the mean trajectory; skill: held-out skill of L; p: temperature-surrogate test of L (descriptive). Bottom row: broadband R^2 and skill as medians over the six indices, p for the group median, octave-band values as medians over all 48 configurations. Octave bands: median and best over the eight bands.

	Broadband 64–16384 Hz			Octave bands		
Index	R^2	skill	p	median R^2	median skill	best skill
ACI	0.59	0.26	0.208	0.40	0.16	0.45
AEI	0.61	0.30	0.205	0.28	0.08	0.31
log band energy	0.27	0.09	0.344	0.70	0.40	0.60
spectral entropy	0.51	0.20	0.129	0.34	0.07	0.28
spectral flatness	0.57	0.24	0.069	0.35	0.07	0.27
temporal entropy	0.49	0.21	0.252	0.41	0.16	0.41
median	0.54	0.22	0.107	0.36	0.12	–

S24 Mass and moisture balance: results

Masses, water fractions and dry-mass losses per bucket (Section S15) are listed in Table S4.

Table S4: Mass and moisture balance per bucket (Section S15). Net masses: bucket readings minus tare (mean of the Monte Carlo draws). Water fraction at the start: 0.65 for all buckets. Dry-mass loss in % of the initial dry mass, mean ± SD over 200 000 Monte Carlo draws, by the direct and the retained-water estimate; pooled: loss of the five buckets together, with 95% Monte Carlo interval.

	Net mass (kg)		Water fraction	Dry-mass loss (%)	
Bucket	start	end	end	direct	retained water
A	5.585	5.405	0.697	17.1 ± 2.5	14.6 ± 5.3
B	5.676	5.436	0.710	21.5 ± 2.4	17.4 ± 5.1
C	5.028	4.788	0.721	25.0 ± 2.4	20.9 ± 5.5
D	5.385	5.105	0.735	29.1 ± 2.6	26.1 ± 5.7
E	4.885	4.645	0.725	26.0 ± 2.5	22.0 ± 5.7
Pooled				23.6 (20.8–26.3)	20.1 (14.1–26.3)

Part C: Supplementary Analyses

S25 Residual diagnostics

Residuals of the fits to the mean trajectory were examined for autocorrelation with the lag-1 correlation and a Ljung–Box test at lag 5 (Ljung and Box, 1978). For the nonlinear measures, the median lag-1 correlation was 0.51 for time-only, 0.52 for temperature-only and 0.24 for L. The Ljung–Box test had $p < 0.05$ in 69%, 56% and 25% of configurations. The corresponding values for the conventional measures were 0.32, 0.35 and 0.23 (40%, 33% and 19%). Under L, the configurations with remaining autocorrelation concentrated at 2048–8192 Hz (Table S7), one of the two frequency ranges in which NP gained most over L (main text, Section 3.5). L therefore removed much, but not all, of the serial structure left by a time trend. In some configurations, this remaining structure was shared by the buckets (main text, Section 3.5). Because residuals are serially ordered and the 80 trajectories share recordings, these p-values were treated as diagnostics rather than pass/fail tests.

S26 Signal-level IAAFT surrogates

These surrogates test the recordings, not the temperature course. They ask whether the nonlinear measures detect temporal structure in the sound that a linear process would not produce.

S26.1 Window selection and series paths

One of the 40 eligible 15 s windows was selected uniformly for each recording with a deterministic filename-based seed. The same window start was used in every octave. Each measure was evaluated using its main-analysis input series, quantiser and definition.

Surrogates were generated from the band-filtered signal of each window. For the nonlinear measures, the RMS series and the measures were then calculated identically from the observed and the surrogate signal. The conventional measures were calculated from the surrogate signal directly. Observed and surrogate values differed in 28 of 32 nonlinear (main text, Section 3.1) and in 24 of 48 conventional configurations, with 95% block-bootstrap intervals excluding zero (Fig. S8). The median absolute effect of the conventional measures was 0.06 standard deviations.

Surrogates of the RMS series itself would be the more direct choice but are not a valid test here. A control on synthetic linear signals showed why. Five 15 s signals at 48 kHz, each a sum of eight independent Gaussian white-noise processes passed through linear one-octave band-pass filters, were analysed with the same bands, RMS windows, quantisers and IAAFT settings. RSE_4, LZC78 and RSR still differed systematically between observed and surrogate RMS series (same sign in 40, 38 and 38 of 40 band series), because the RMS series of a linear Gaussian signal is a nonlinear transform of that signal.

The same linear control (40 accepted band series per measure) showed no such bias for the signal surrogates used here. Observed and surrogate values of the nonlinear measures did not differ systematically in two-sided sign tests (RSE_4 $p = 1.00$, LZC78 $p = 0.52$,

PE $p = 0.87$, RSR $p = 1.00$). The median raw-unit differences were close to zero (RSE_4 −0.00002, LZC78 1.5, PE −0.0001, RSR 0.000002). In the experimental recordings, the corresponding median differences were 0.0055, −23, −0.0025 and 0.0012, about ten times larger or more. The observed effects therefore indicate temporal structure that a stationary linear process with the same spectrum and amplitude distribution does not reproduce. Because IAAFT surrogates are stationary, non-stationarity within the 15 s windows is an alternative source of this structure besides nonlinear dynamics. The effects were largest below 1024 Hz and smallest in the two highest octaves, where experimental and linear differences were of similar size.

S26.2 Surrogate generation and convergence

IAAFT began with a random permutation of the observed series and alternated between imposing the observed Fourier magnitudes and rank-matching to the sorted observed amplitudes (Schreiber and Schmitz, 1996). Up to five seeds were tried, the attempt with the lowest relative spectral error $E = \| |\mathrm{FFT}(\text{surrogate})| - |\mathrm{FFT}(\text{observed})| \| / \| |\mathrm{FFT}(\text{observed})| \|$ was kept, and a comparison was excluded when E exceeded 2.5%. This excluded 166 of the 1 200 recording-band series of the nonlinear measures (14%) and 165 of 1 200 for the conventional measures. For the nonlinear measures, the share ranged from none at 8192–16384 Hz to 32% at 512–1024 Hz, and most exclusions fell in 256–2048 Hz.

S26.3 Effects and uncertainty

For recording i in bucket s, the paired effect was $d_{si} = (\text{observed}_{si} - \text{surrogate}_{si})/\mathrm{SD}_{s,\text{main}}$, where $\mathrm{SD}_{s,\text{main}}$ was the sample standard deviation used for the main standardisation of that bucket and configuration. Within each bucket and measure-band cell, the median of all spectrally valid d_{si} was calculated. The reported cell effect is the unweighted mean of the five bucket medians (Fig. S8). Uncertainty used 5 000 paired circular moving-block bootstrap draws within each bucket, with blocks of four consecutive recordings and wrap-around at the trajectory end (Politis and Romano, 1992). Percentile 95% intervals were reported. IAAFT preserves the amplitude spectrum, so effects on log band energy (zero by construction), spectral entropy and spectral flatness, which are functions of it, are small by design.

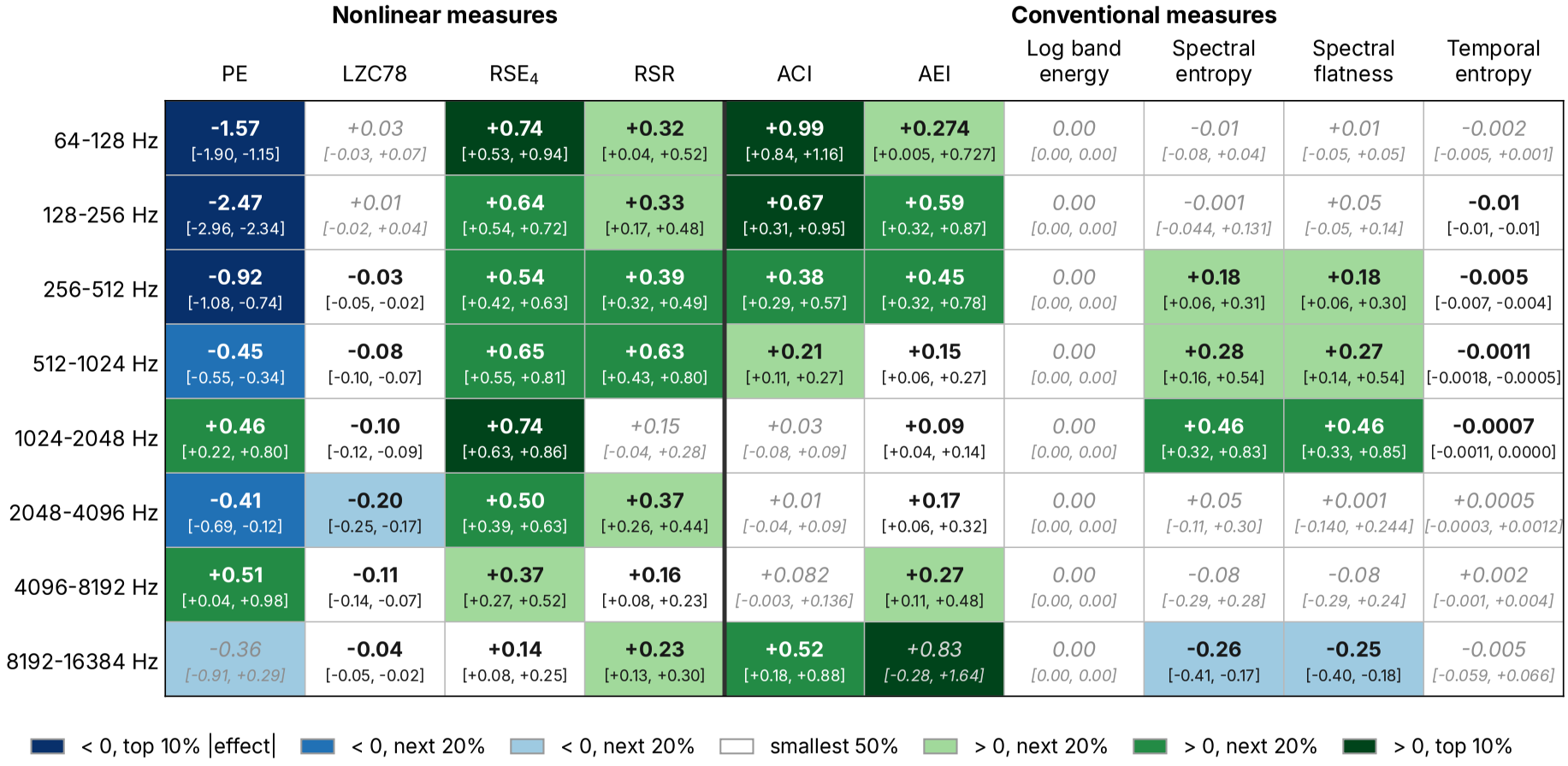


Figure S8: Signal-level IAAFT effect for all measures against the band-signal surrogate, in standard deviations of the main analysis (observed minus surrogate). For the nonlinear measures, the RMS series was computed from the surrogate signal. The conventional measures were computed from the surrogate signal directly. Each cell shows the effect (mean of the five bucket medians, upper number) and its paired 95% block-bootstrap interval (lower numbers). Shading ranks the absolute effects of all 80 cells of this table (largest 10% darkest, then 20% and 20%, smallest 50% white). Green marks positive and blue negative effects. Grey italic text marks cells whose interval includes zero. Log band energy is zero by construction. The sign shows whether the observed value lies above or below the surrogate, not whether it carries more or less structure.

S27 Further checks

All checks used the data of Section S11. The cross-validated checks also used its folds and skill.

S27.1 Own versus mean temperature

L and temperature-only were cross-validated with the mean temperature of the four training buckets in place of each bucket's own temperature, for the training buckets and for the held-out bucket, so that no bucket-specific temperature entered the prediction. The median skill of L was then 0.480 for the nonlinear and 0.122 for the conventional configurations, against 0.485 and 0.124 with each bucket's own temperature. The median paired differences were 0.004 and 0.002, and the largest absolute difference was 0.020. The buckets differed from the mean course by a median of 0.16 °C (at most 1.3 °C), against a range of the mean course of 26.2–39.4 °C.

S27.2 Temperature differences between buckets

At each occasion, the five buckets were recorded at nearly the same elapsed time, so differences between them are free of the shared time course. Temperature and standardised values were centred on their occasion means across buckets. For every configuration, L predicts the centred value of a bucket as $(d + e\,C_i)$ times its centred temperature, with d and e from the fit to the mean trajectory. The ratio γ of observed to predicted differences was pooled over all 80 configurations as $\sum xy / \sum x^2$, with x the predicted and y the observed centred value. The temperature deviations were permuted between the buckets of each occasion (100 000 permutations, applied jointly to all configurations), and p is the share of permutations with a γ at least as large as the observed one. The 150 deviations were small, with a median of 0.16 °C, a standard deviation of 0.36 °C and a maximum of 1.1 °C. The observed differences followed the prediction of L with $\gamma = 1.03$ ($p = 0.015$; permutation 95th percentile 0.80), and the sign matched the prediction in 80% of the configurations. The shared temperature course contains the predictive information (previous subsection), while these differences are too small to improve prediction. The test does not distinguish a temperature effect from a common cause, such as a warmer bucket also being more active.

S27.3 Linear time term

With an additional linear time term, the median held-out skill of L was 0.493 for the nonlinear and 0.145 for the conventional configurations, against 0.485 and 0.124 without it.

S27.4 Skill by phase

The skill of a fold was also computed separately over the heating occasions of the held-out bucket (measurements 1–5) and over its cooling occasions, from the same predictions (Table S5). The shares of SSE_0 and of the part explained by L that fall on heating occasions show that the heating phase is predicted well but on few values, so the overall skill is dominated by the cooling phase. Both four-parameter models predicted heating well. The advantage of L over $\mathrm{L}_{\mathrm{time}}$ lay mainly in the cooling phase.

S27.5 Heating-occasion jackknife

In L, the intercept and the heating slope d are determined by the heating occasions alone, because the cooling branch has its own offset and slope. L was thus refitted to the mean trajectory five times, each time without one of measurements 1–5. The sign of the cooling offset b was unchanged in 94% of the nonlinear and 92% of the conventional configurations, that of the slope change e in 84% and 90%, and that of the heating slope d in 81% and 60%.

S27.6 Difference between the branches

The cooling offset b is the difference between the cooling and the heating branch of L at the arbitrary centring temperature of 30 °C. The difference $\Delta(T) = b + e\,(T - 30)$ was also evaluated across the temperature range covered by both phases of the mean course (28.0–38.0 °C) and at its midpoint (33 °C), with the fit to the mean trajectory, the heating-occasion jackknife and the Bayesian-bootstrap draws. At 33 °C, the median absolute difference between the branches was 0.71 standard deviations for the nonlinear and 0.43 for the conventional configurations. Its 95% interval excluded zero at 33 °C in 28 of 32 nonlinear and 38 of 48 conventional configurations, at some temperature within 28–38 °C in 30 and 45, and at every temperature of this range in 16 and 8. Per configuration, the interval excluded zero over a median of 96% (nonlinear) and 73% (conventional) of the range. The branches crossed within the range in 8 nonlinear and 20 conventional configurations, so there the phases differed mainly in slope. In the jackknife, the sign of the difference at 33 °C was unchanged in 30 of 32 nonlinear and 43 of 48 conventional configurations.

S27.7 Session time and mains hum

L was extended by a session-time or a mains-hum indicator as a fifth term. The session indicator was 1 for afternoon (13:00) and 0 for evening (21:00) sessions, and 0.5 for the baseline, which started at 18:00. Mains hum was scored per recording from the same 600 s excerpts and 15 s windows as the measures. In every window, the peak of the Hann-windowed power spectrum between 49 and 51 Hz was compared with the median power between 30–46 and 54–70 Hz. The signal-to-noise ratio was bimodal, and a recording was scored as hum present when more than half of its windows exceeded 25 dB, which applied to 53% of the recordings. Hum entered the fit to the mean trajectory as the share of buckets with hum per occasion and the cross-validation as the hum of each bucket's own recording. Neither term improved the nonlinear median held-out skill. No configuration changed by more than 0.05 in either direction, and losses outnumbered gains (Table S6). Because the 50 Hz line itself lies below the analysed bands, an effect of hum on the measures could only arise through its harmonics (100–250 Hz in the two lowest bands). The hum term thus tests all harmonics together.

S27.8 Without the highest band

At 8192–16384 Hz, band energy varied by only about 1 dB, so a small temperature response of the sensor could affect this band (main text, Section 3.6). The main comparisons were repeated without it (28 nonlinear and 42 conventional configurations), with the held-out skills of Section S11 and the same 100 000 temperature surrogates (Table S8).

The median held-out skill of L for the nonlinear measures was almost unchanged (0.48), L remained the best of the four temperature and time models, and its surrogate test gave $p = 0.00002$ (0.00003 with all bands). The conventional indices again did not separate from the surrogates.

S27.9 Level-invariant control

Changes in sound attenuation by the material are expected to act within one octave band mainly on the absolute level, while faunal sounds also change the temporal pattern (main text, Section 3.3). LZC78, RSE_4 and RSR depend on the absolute level of the band envelope through the quantiser (Section S6). In a descriptive control, this quantiser was made level-invariant. For every recording, band and alphabet, the quantiser was fitted from the RMS envelope of this recording alone, with the same 4 000 evenly spaced support values and the same 1st–99th percentile rule, instead of one quantiser per bucket for all occasions. The windows, the standardisation, the models, the cross-validation and the Bayesian bootstrap were unchanged, and no surrogate test was applied. PE depends only on the rank order of consecutive envelope values and was not recomputed. Two variants served as checks: a quantiser fitted from each 15 s window itself, and the quantiser per recording evaluated only in the two windows that held the median of the 40 window values in the main analysis (the two middle ranks).

With the quantiser per recording, the nonlinear median held-out skill of L fell from 0.48 to 0.17, that of the time-only model from 0.33 to 0.09, and the R^2 of the fit to the mean trajectory from 0.81 to 0.42 (Table S9). L remained better than the time-only model in 29 of 32 configurations (30 in the main analysis), and both variants gave similar values. PE was unaffected (held-out skill 0.31). The heating-cooling terms persisted at a smaller size. The 95% Bayesian-bootstrap interval of the cooling offset b excluded zero in 26 (28 in the main analysis), that of the heating slope d in 19 (19) and that of the slope change e in 24 (22) of 32 nonlinear configurations. The median difference between the branches at 33 °C was 0.40 standard deviations (0.71), its interval excluded zero at 33 °C in 22 of 32 configurations (28), and the branches crossed within the range in 17 (8). Scored by phase, the nonlinear median skill of L was 0.42 on heating and 0.11 on cooling occasions (0.70 and 0.42). Without the absolute level, short-term variability increased. The standard deviation of the differences between consecutive occasions of the mean trajectory, relative to that of the trajectory, rose from a median of 0.51 to 0.86 in the 24 configurations that depend on the quantiser. It increased in 19 of them, and for PE the median was 0.72.

The variation left by L followed that of PE more consistently once the level was removed (Table S10). At 1–8 kHz, the absolute correlation of the residuals of LZC78, RSE_4 and RSR with those of PE in the same band was between 0.65 and 0.89 (0.01 and 0.93 in the main analysis). At 8192–16384 Hz, it was low with both quantisers, 0.08–0.22 per recording and 0.01–0.10 in the main analysis. Fig. S9 shows RSR at four octave bands (a) and its coefficients (b), and corresponds to main-text Fig. 1 (time panels, other bands), main-text Fig. 4 (coefficients) and main-text Fig. 6 (NP). The multi-day structure around days 8–10, seen in PE at 4096–8192 Hz (main text, Section 3.5), is visible in RSR at 4096–8192 Hz once the level is removed.

The control can be read in one direction only. A persistent effect cannot be explained by attenuation of the material alone. A reduced effect is inconclusive, because the level also carries faunal information. The quantiser per recording removes the absolute level and

the dynamic range within a band, so the control is not a complete normalisation of the signal.

Table S5: Held-out skill by phase: medians over the configurations of each group, over all occasions and separately over heating (measurements 1–5) and cooling occasions (6–31) of the held-out buckets (23 and 127 values over the five folds). Bottom rows: share of SSE_0 and of the part explained by L ($SSE_0 - SSE$) that falls on heating occasions (medians over configurations).

	Nonlinear (32)			Conventional (48)		
Model	all	heating	cooling	all	heating	cooling
time-only	0.33	0.31	0.29	0.07	0.17	0.03
temperature-only	0.30	0.18	0.41	0.07	-0.00	0.07
L_{time}	0.40	0.71	0.30	0.08	0.35	0.03
L	0.48	0.70	0.42	0.12	0.39	0.08
share of SSE_0 (heating)		21%			8%	
share of explained SS (heating, L)		32%			33%	

Table S6: Session time (afternoon/evening) and mains hum as an additional term of L (Section S27). Δ: median of L plus the term minus median of L over the configurations of a group (skill: held-out skill; R^2: fit to the mean trajectory). Gain/loss: configurations whose held-out skill rose or fell. Max/min: largest single-configuration gain and loss.

Covariate	Group	Δ skill	ΔR^2	gain/loss	max/min
afternoon/evening	nonlinear	-0.001	$+0.000$	10/22	$+0.00$ / -0.02
afternoon/evening	conventional	$+0.014$	$+0.057$	18/30	$+0.03$ / -0.03
mains hum	nonlinear	-0.006	$+0.002$	11/21	$+0.03$ / -0.02
mains hum	conventional	-0.002	$+0.024$	23/25	$+0.03$ / -0.05

Table S7: Configurations whose residuals in the fit to the mean trajectory had a Ljung–Box $p < 0.05$ (lag 5; Section S25), per octave band, for time-only (time), temperature-only (T) and L; nonlinear: 4 and conventional: 6 configurations per band.

	Nonlinear (32)			Conventional (48)		
Band	time	T	L	time	T	L
64–128 Hz	1/4	1/4	0/4	1/6	2/6	0/6
128–256 Hz	3/4	3/4	1/4	2/6	2/6	0/6
256–512 Hz	4/4	3/4	2/4	1/6	1/6	0/6
512–1024 Hz	3/4	3/4	0/4	1/6	0/6	0/6
1024–2048 Hz	2/4	2/4	1/4	0/6	0/6	0/6
2048–4096 Hz	3/4	3/4	3/4	6/6	3/6	3/6
4096–8192 Hz	4/4	3/4	1/4	4/6	4/6	4/6
8192–16384 Hz	2/4	0/4	0/4	4/6	4/6	2/6

Table S8: Main comparisons with all eight octave bands and without the 8192–16384 Hz band: median held-out skill of the models over the configurations of a group, number of configurations in which L predicted better than time-only / temperature-only / L_{time}, and temperature-surrogate p of L (same 100 000 surrogates; bold: primary test).

Group	Bands	n	time-only	T-only	L_{time}	L	NP	L better	p (L)
nonlinear	all	32	0.33	0.30	0.40	0.48	0.50	30/29/26	**0.00003**
nonlinear	without 8–16 kHz	28	0.32	0.29	0.39	0.48	0.49	26/25/22	0.00002
conventional	all	48	0.07	0.07	0.08	0.12	0.18	42/40/41	0.206
conventional	without 8–16 kHz	42	0.07	0.07	0.07	0.11	0.16	36/35/36	0.219

Table S9: Quantisers fitted per bucket (main analysis), per recording (control), per 15 s window, and per recording in the two median windows only. Medians over the nonlinear configurations (including PE, which is unchanged) and over LZC78, RSE_4 and RSR: held-out skill of the time-only model (time) and of L, R^2 of L in the fit to the mean trajectory, and the number of configurations in which L predicted better than time-only. No surrogate test was applied.

	Nonlinear (32)				LZC78, RSE_4, RSR (24)			
Quantiser	time	L	R^2 of L	L > time	time	L	R^2 of L	L > time
Quantiser per bucket (main analysis)	0.33	0.48	0.81	30/32	0.34	0.51	0.84	23/24
Quantiser per recording (control)	0.09	0.17	0.42	29/32	0.09	0.16	0.39	22/24
Quantiser per 15 s window	0.08	0.17	0.37	31/32	0.08	0.17	0.34	24/24
Per recording, two median windows only	0.09	0.17	0.42	27/32	0.09	0.16	0.40	21/24

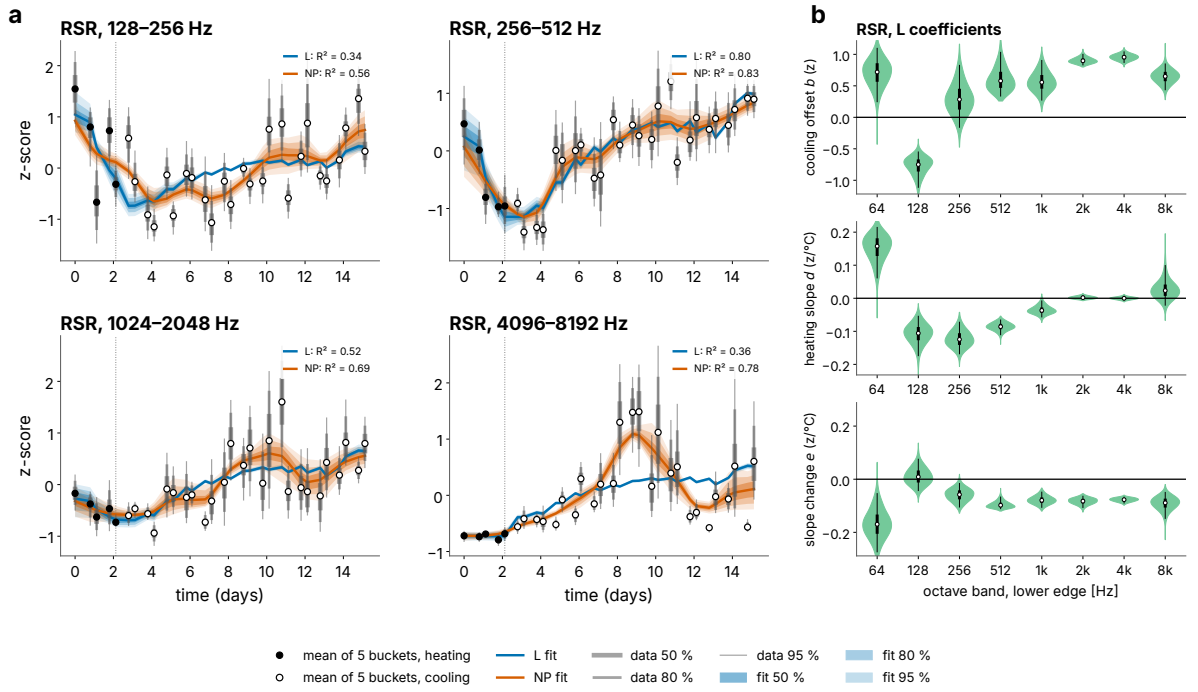


Figure S9: RSR with quantisers fitted per recording (level-invariant control). (a) Mean of buckets A–E over time at 128–256, 256–512, 1024–2048 and 4096–8192 Hz, with L (blue) and the data-driven shared curve NP (orange) and their 50, 80 and 95% intervals over the Bayesian bootstrap draws. Points as in main-text Fig. 1; R^2: fit to the mean trajectory. NP is more flexible than L, so its R^2 is not comparable. (b) Coefficients of L by octave band (violins as in main-text Fig. 4). Without the absolute level, short-term variability increased and effect sizes decreased, but the overall pattern persisted.

Table S10: Correlation of the residuals of L (fit to the mean trajectory) of LZC78, RSE_4 and RSR with those of PE in the same octave band, with quantisers fitted per bucket (main analysis) and per recording.

	Quantiser per bucket			Quantiser per recording		
Band (Hz)	LZC78	RSE_4	RSR	LZC78	RSE_4	RSR
64–128	−0.29	−0.32	−0.56	+0.28	−0.62	−0.73
128–256	−0.42	−0.05	+0.01	+0.54	−0.56	−0.57
256–512	−0.87	+0.74	+0.61	+0.41	−0.55	−0.67
512–1024	−0.92	+0.69	+0.46	+0.56	−0.69	−0.82
1024–2048	−0.93	−0.48	+0.01	+0.80	−0.89	−0.89
2048–4096	−0.61	−0.68	−0.58	+0.65	−0.67	−0.66
4096–8192	−0.49	−0.48	−0.55	+0.70	−0.72	−0.70
8192–16384	−0.10	+0.01	+0.06	+0.09	−0.08	−0.22

References

Bandt, C., Pompe, B., 2002. Permutation entropy: a natural complexity measure for time series. Physical Review Letters 88, 174102. doi:10.1103/PhysRevLett.88.174102.

Brown, P., 2015. Humidity, hay moisture and harvest management, in: Proceedings of the 2015 Western States Alfalfa and Forage Symposium, Reno, Nevada. URL: https://alfalfasymposium.ucdavis.edu/+symposium/2015/index.aspx. 2–4 December 2015; accessed 29 October 2026.

Deutscher Wetterdienst, 2026. Hourly air-temperature and relative-humidity observations, station 03284 Michelstadt, 22–26 June 2026. URL: https://opendata.dwd.de/climate_environment/CDC/observations_germany/climate/hourly/air_temperature/. Open data, Climate Data Center; accessed 29 October 2026.

EFSA Panel on Dietetic Products, Nutrition, and Allergies, 2010. Scientific opinion on dietary reference values for water. EFSA Journal 8, 1459. doi:10.2903/j.efsa.2010.1459.

Eisenhauer, J., 2026a. Hearing the heat: analysis code, version 1.2.0. Zenodo. https://doi.org/10.5281/zenodo.23959730.

Eisenhauer, J., 2026b. Hearing the heat: soil probe recordings of rapid organic decomposition (150 x 10 min), version 1.0.0. Zenodo. https://doi.org/10.5281/zenodo.23891122.

Hurlbert, S.H., 1984. Pseudoreplication and the design of ecological field experiments. Ecological Monographs 54, 187–211. doi:10.2307/1942661.

Johnson, K., 2022. Environmental conditions affect time to safe hay baling. Pest and Crop Newsletter URL: https://extension.entm.purdue.edu/newsletters/pestandcrop/article/environmental-conditions-affect-time-to-safe-hay-baling-3/. Issue 2022.10, 27 May 2022, Purdue University Extension; table source: NRAES-5, Silage and Hay Preservation; accessed 29 October 2026.

KERN & Sohn GmbH, 2026. Technical data sheets: HCB 50K20 hanging balance and EMB 5.2K1 precision balance. Technical Report. KERN & Sohn GmbH. https://kern-sohn.com/cosmoshop/default/pix/a/media/HCB%2050K20/TD_HCB+50K20_en.pdf and https://igelmam.kern-sohn.com/media/pk2ntk1k/emb-52k1-en.pdf; accessed 29 October 2026.

Ljung, G.M., Box, G.E.P., 1978. On a measure of lack of fit in time series models. Biometrika 65, 297–303. doi:10.1093/biomet/65.2.297.

Nadaraya, E.A., 1964. On estimating regression. Theory of Probability and Its Applications 9, 141–142. doi:10.1137/1109020.

Pieretti, N., Farina, A., Morri, D., 2011. A new methodology to infer the singing activity of an avian community: the acoustic complexity index (ACI). Ecological Indicators 11, 868–873. doi:10.1016/j.ecolind.2010.11.005.

Politis, D.N., Romano, J.P., 1992. A circular block-resampling procedure for stationary data, in: LePage, R., Billard, L. (Eds.), Exploring the Limits of Bootstrap. Wiley, New York, pp. 263–270.

Richard, T.L., Hamelers, H.V.M., Veeken, A., Silva, T., 2002. Moisture relationships in composting processes. Compost Science & Utilization 10, 286–302. doi:10.1080/1065657X.2002.10702093.

Roberts, D.R., Bahn, V., Ciuti, S., Boyce, M.S., Elith, J., Guillera-Arroita, G., Hauenstein, S., Lahoz-Monfort, J.J., Schröder, B., Thuiller, W., Warton, D.I., Wintle, B.A., Hartig, F., Dormann, C.F., 2017. Cross-validation strategies for data with temporal, spatial, hierarchical, or phylogenetic structure. Ecography 40, 913–929. doi:10.1111/ecog.02881.

Rubin, D.B., 1981. The Bayesian bootstrap. The Annals of Statistics 9, 130–134. doi:10.1214/aos/1176345338.

Schreiber, T., Schmitz, A., 1996. Improved surrogate data for nonlinearity tests. Physical Review Letters 77, 635–638. doi:10.1103/PhysRevLett.77.635.

Sueur, J., Aubin, T., Simonis, C., 2008a. Seewave, a free modular tool for sound analysis and synthesis. Bioacoustics 18, 213–226. doi:10.1080/09524622.2008.9753600.

Sueur, J., Aubin, T., Simonis, C., 2025. seewave: sound analysis and synthesis, R package version 2.2.4. https://CRAN.R-project.org/package=seewave.

Sueur, J., Pavoine, S., Hamerlynck, O., Duvail, S., 2008b. Rapid acoustic survey for biodiversity appraisal. PLoS ONE 3, e4065. doi:10.1371/journal.pone.0004065.

Villanueva-Rivera, L.J., Pijanowski, B.C., 2018. soundecology: soundscape ecology, R package version 1.3.3. https://CRAN.R-project.org/package=soundecology.

Villanueva-Rivera, L.J., Pijanowski, B.C., Doucette, J., Pekin, B., 2011. A primer of acoustic analysis for landscape ecologists. Landscape Ecology 26, 1233–1246. doi:10.1007/s10980-011-9636-9.

Watson, G.S., 1964. Smooth regression analysis. Sankhyā: The Indian Journal of Statistics, Series A 26, 359–372.

Ziv, J., Lempel, A., 1978. Compression of individual sequences via variable-rate coding. IEEE Transactions on Information Theory 24, 530–536. doi:10.1109/TIT.1978.1055934.